A Critical Validation of Density Functional and Coupled-Cluster Approaches for the Calculation of EPR Hyperfine Coupling Constants in Transition Metal Complexes

Markéta Munzarová and Martin Kaupp*

Max-Planck-Institut für Festkörperforschung, Heisenbergstrasse 1, D-70569 Stuttgart, Germany

Received: July 7, 1999; In Final Form: September 27, 1999

The performance of various density functional approaches for the calculation of electron paramagnetic resonance (EPR) hyperfine coupling constants in transition metal complexes has been evaluated critically by comparison with experimental data and high-level coupled-cluster results for 21 systems, representing a large variety of different electronic situations. While both gradient-corrected and hybrid functionals allow the calculation of isotropic metal hyperfine coupling constants to within ca. 10−15% for the less critical cases (e.g., ScO, TiN, TiO, VO, MnO, MnF), none of the functionals investigated performs well for all complexes. Gradient-corrected functionals tend to underestimate the important core−shell spin polarization. While this may be improved by exact-exchange mixing in some cases, the accompanying spin contamination may even lead to a deterioration of the results for other complexes. We also identify cases, where essentially none of the functionals performs satisfactorily. In the absence of a ”universal functional”, the functionals to be applied to the calculation of hyperfine couplings in certain areas of transition metal chemistry have to be carefully selected. Desirable, improved functionals should provide sufficiently large spin polarization for core and valence shells without exaggerating it for the latter (and thus introducing spin contamination). Coupling anisotropies and coupling constants for ligand nuclei are also discussed. The computationally much more demanding coupled cluster (CCSD and CCSD(T)) methods, which have been applied to a subset of complexes, show good performance, even when a UHF reference wave function is moderately spin-contaminated.

1. Introduction

Electron paramagnetic resonance (EPR) spectroscopy represents one of the most powerful experimental tools for studying the molecular and electronic structure of compounds containing unpaired electrons. Since the early days of this technique, a large number of EPR spectra for transition metal complexes have been measured. A wealth of experimental data on electronic g-tensors and hyperfine coupling constants (HFCCs) is thus available.[1−8] Quantitative theoretical studies of HFCCs have, however, concentrated largely on organic molecules or on other light main group systems. This is understandable, as the accurate inclusion of electron-correlation effects is mandatory for quantitative calculations of electron−nuclear hyperfine interactions. To achieve this in traditional post-Hartree−Fock ab initio calculations is far from trivial, and such treatments are not easily applicable to larger transition metal complexes. CAS−SCF and MR−SDCI calculations have been done on ScO, TiN, and VN by Mattar et al.,[9−11] as well as on VO_x ($x = 1, 2, 3$) by Knight et al.[12] To our knowledge, no other transition metal systems have been treated at comparable levels.

Recent developments in density functional theory (DFT) do in principle provide an alternative, as DFT includes electron correlation approximately, at moderate computational cost. A number of Kohn−Sham DFT studies on transition metal HFCCs have appeared, using local-spin-density approximations (LSDA), generalized-gradient approximations (GGA), as well as hybrid functionals including exact exchange. Hyperfine parameters have been computed for VN by Mattar and Doleman,[11] for TiN and TiO by Engels et al.,[13] for CuC_2H_2 and Cu(CO) by Barone et al.,[14,15] for a ruthenium complex by Aarnts et al.,[16] for TiF_3 by Belanzoni et al.[17,18] and by van Lenthe et al.,[19] and for a series of molybdenum(V) oxyhalide anions by Swann and Westmoreland.[20] During the course of the present study, Knight et al. reported DFT results on MO (M = Sc, Y, La).[21] A number of earlier calculations employed the X_α method.[22−24] Reasonable agreement between experiment and theory for the isotropic HFCCs has been found when significant metal s-character in the singly occupied molecular orbitals (SOMOs) leads to a dominance of direct contributions to the spin density at the nucleus. The description is expected to be considerably more complicated when spin-polarization effects become large, a situation that should apply for many transition metal systems.[1]

In the studies mentioned, only a limited number of exchange−correlation functionals and basis sets have been employed, and only a relatively small set of molecules and electronic structure situations was encompassed. Further systematic studies are thus needed, if one wants to be able to judge in detail the ability of the available DFT approaches to describe HFCCs for transition metal systems. Here we present a critical validation study, including twenty-one first-row transition metal complexes and eight different state-of-the-art exchange−correlation potentials ν_{xc}. Throughout this work, we have learned much about the mechanisms of spin polarization and related phenomena for HFCCs in transition metal complexes. These interpretational aspects will be covered in more detail elsewhere[25] (including numerical results), but will be touched upon briefly in this work whenever needed for an understanding of the performance of different functionals.

After outlining roughly the nonrelativistic theoretical formalism of hyperfine couplings in section 2 (mainly to connect to the rather different types of experimental information available), we will discuss problems connected with the selection of

---

* Corresponding author e-mail: kaupp@vsibm1.mpi-stuttgart.mpg.de

10.1021/jp992303p CCC: $18.00

experimental data (section 3). Information on molecular structures, basis sets, and theoretical approaches used is given in section 4. After a description of coupled cluster results for a subset of the complexes (section 5), which we employ as reference data, basis set effects are examined in section 6. Then the performance of different exchange−correlation functionals is compared systematically for the metal HFCCs (section 7), followed by a brief discussion of ligand HFCCs (section 8). A number of general conclusions are provided in section 9.

2. Theoretical Formalism

The theory of EPR hyperfine couplings is covered in detail in text books,[1,3−8,26] and we summarize only those points which are important for the comparison between computed and experimental quantities. The hyperfine coupling parameters describe the interactions of unpaired electrons with various magnetic nuclei. The 3 × 3 hyperfine interaction tensor A can be separated into its isotropic and anisotropic (dipolar) components.[6] In the first-order approximation (neglecting spin−orbit effects; cf. discussion in section 4), isotropic hyperfine splittings $A_{\mathrm{iso}}(\mathrm{N})$ are equal to the Fermi contact term A_{FC} and they are related to the spin densities $\rho^{\alpha-\beta}(R_{\mathrm{N}})$ at the corresponding nuclei by[4]

$$A_{\mathrm{iso}}(\mathrm{N}) = A_{\mathrm{FC}} = \frac{4\pi}{3}\beta_{\mathrm{e}}\beta_{\mathrm{N}}g_{\mathrm{e}}g_{\mathrm{N}}\langle S_{\mathrm{Z}}\rangle^{-1}\rho_{\mathrm{N}}{}^{\alpha-\beta} \qquad (1)$$

where β_{e} is the Bohr magneton, β_{N} the nuclear magneton, g_{e} the free electron g-value (2.002 319 31). The g-value of the nucleus N is given by $g_{\mathrm{N}} = \mu_{\mathrm{N}}/I_{\mathrm{N}}$ (μ_{N} is the nuclear magnetic moment of nucleus N in units of β_{N}, and I_{N} is the total nuclear spin for that nucleus). $\langle S_{\mathrm{Z}}\rangle$ is the expectation value of the *z*-component of the total electronic spin. The spin density $\rho_{\mathrm{N}}{}^{\alpha-\beta}$ at the position of nucleus N (R_{N}) can be expressed as:

$$\rho_{\mathrm{N}}{}^{\alpha-\beta} = \sum_{\mu,\nu} P_{\mu,\nu}^{\alpha-\beta}\langle\phi_\mu|\delta(R_{\mathrm{N}})|\phi_\nu\rangle \qquad (2)$$

where $P_{\mu,\nu}^{\alpha-\beta}$ is the spin density matrix. We will in the following abbreviate $\rho_{\mathrm{N}}{}^{\alpha-\beta}$ by ρ_{N}.

The components T_{kl} of the anisotropic tensor are in the first-order approximation given by[31]

$$T_{kl}(\mathrm{N}) = \frac{1}{2}\beta_{\mathrm{e}}\beta_{\mathrm{N}}g_{\mathrm{e}}g_{\mathrm{N}}\langle \mathrm{S}_{\mathrm{Z}}\rangle^{-1}\sum_{\mu\nu} P_{\mu,\nu}^{\alpha-\beta} \times \langle\phi_\mu|r_{\mathrm{N}}^{-5}(r_{\mathrm{N}}^2\delta_{kl} - 3r_{\mathrm{N},k}r_{\mathrm{N},l})|\phi_\nu\rangle \qquad (3)$$

where $r_{\mathrm{N}} = r - R_{\mathrm{N}}$. T is always traceless and may be brought to diagonal form. For magnetic nuclei with an electronic environment of axial symmetry (i.e., those located on an at least 3-fold symmetry axis), it has the form ($-A_{\mathrm{dip}}$, $-A_{\mathrm{dip}}$, $2A_{\mathrm{dip}}$), where A_{dip} is the so-called dipolar coupling constant. From the experimental tensor components ($A_\perp$, $A_\perp$, $A_{||}$), A_{iso} and A_{dip} may then be extracted via $A_{\mathrm{iso}} = (A_{||} + 2A_\perp)/3$, $A_{\mathrm{dip}} = (A_{||} - A_\perp)/3$. Another terminology is used in gas-phase spectroscopy studies.[30] The high-resolution spectra of linear molecules can be described in terms of five parameters (*a, b, c, d, e*), of which *b* and *c* are related to A_{iso} and A_{dip} as $A_{\mathrm{iso}} = (b + c/3)$ and $A_{\mathrm{dip}} = c/3$.

All transition metal nuclei in the present study are at sites of axial symmetry. Although this is not the case for all ligands, experimentalists in the field prefer to use the "A_{dip}" terminology, even if it is not justified by symmetry. This is often due to the fact that the dipolar ligand splittings are small, and two different "perpendicular" components are not observed in the spectra (at least for complexes such as those considered here, where the unpaired spin density is mainly localized on the metal). See section 4 for comments on spin−orbit corrections to the hyperfine couplings.

3. Selection of Experimental Data

The selection of the molecules used in this study was determined mainly by the availability of experimental data on small systems having a well-resolved hyperfine structure for the metal and, if possible, also for the ligands. We have included examples for all first-row transition metals. Some pairs of isoelectronic molecules have been selected to compare different transition metals in similar electronic surroundings. In the following we will comment on the interpretation of the measured data and on the expected accuracy of different experimental techniques.

Gas-Phase Data. For all diatomic oxides and nitrides, and for MnH, literature hyperfine parameters from high-resolution gas-phase molecular spectroscopy have been used. The relative positions of the energy levels were obtained either directly by monitoring of the absorption/emission (”pure” microwave rotational spectroscopy) or indirectly (through fluorescence or molecular beam deflection).[30] The hyperfine parameters have been determined from the analysis of the level splittings. The accuracy of such measurements is usually very high, sometimes in the kHz range for microwave optical double resonance.[27−29]

In most of the gas-phase investigations, the interactions between molecules represent relatively small perturbations which usually affect only the widths of the spectral lines; in molecular beam studies such interactions are completely absent.[30] This makes the gas-phase data most reliable for comparison with our computed data on isolated molecules. Moreover, in these gas-phase experiments, the sign of the HFCCs is known.

Condensed-Phase EPR Data. For the remaining systems, the hyperfine parameters had to be taken from condensed-phase EPR spectroscopy. Different trapping sites (mostly inert-gas matrices, but also host crystals and frozen solutions) are thus involved. Obviously, the environment can influence the values of the hyperfine parameters, in particular of the isotropic coupling constants,[31] due to both structural and electronical effects. This complicates the comparison of our calculated data with experiment.

In those few cases where EPR results are available on the same complex from both gas- and condensed-phase measurements, the HFCCs differ typically by a few percent, up to ca. 10% in extreme cases. Thus, e.g., the gas-to-matrix shift for $A_{\mathrm{iso}}(\mathrm{V})$ of VO is less than 3% of the absolute value (data available are 798 MHz in Ne matrix,[12] 796 MHz in Ar matrix,[32] and 778 MHz in the gas phase[33]). The situation is similar for ScO (cf. matrix values of 2005−2018 MHz[34,21] vs gas-phase value of 1947 MHz[28] for $A_{\mathrm{iso}}(\mathrm{Sc})$). Larger gas-to-matrix shifts have been found for MnO (7%; cf. 448 MHz in matrix[35] vs 480 MHz in the gas phase[36]) and MnH (11%, see ref 37). For charged species, counterion effects may be considerable and have to be kept in mind as a potential source of errors.

In view of these environmental effects, we cannot aim at a better agreement with condensed-phase experiments than ca. 10−15%. Furthermore, the theoretical values should best be compared with the whole range of accurate experimental data available. This is most important for complexes with very small isotropic coupling constants, since these are particularly sensitive to the influence of the surroundings. We note also that the computed structures do not include any rovibrational corrections. On the other hand, the experimental structures also have to be viewed with some error bars. Structural aspects contribute thus

TABLE 1: Structures Used in the HFCC Calculations[a]

molecule		metal−ligand (intraligand) bond lengths and angles	source[b]
ScO	$C_{\infty v}$	1.667	opt
TiN	$C_{\infty v}$	1.567	opt
TiO	$C_{\infty v}$	1.623	*c*
VN	$C_{\infty v}$	1.567	*d*
VO	$C_{\infty v}$	1.589	*e*
MnH	$C_{\infty v}$	1.731	*f*
MnO	$C_{\infty v}$	1.648	*g*
MnF	$C_{\infty v}$	1.839	opt
CuO	$C_{\infty v}$	1.729	*h*
MnF_2	$D_{\infty h}$	1.811	*i*
TiF_3	D_{3h}	1.780	opt
MnO_3	D_{3h}	1.579	opt
$[Cu(CO)_3]$	D_{3h}	1.796 (1.151)	opt. MP2[j]
$[Cr(CO)_4]^+$	T_d	2.190 (1.122)	opt
$[Mn(CN)_4]^{2-}$	T_d	2.158 (1.133)	*k*
$[Ni(CO)_3H]$	C_{3v}	d(Ni−H) = 1.512, d(Ni−C) = 1.851, d(C−O) = 1.135, ∠(H−Ni−C) = 90.87, ∠(Ni−C−O) = 171.29	opt
$[Co(CO)_4]$	C_{3v}	d(Co−C_{ax}) = 1.875, d(Co−C_{eq}) = 1.847, d$(C-O)_{ax}$ = 1.137, d$(C-O)_{eq}$ = 1.139 ∠(C_{ax}−Co−C_{eq}) = 99.2, ∠(Co−C−O) = 179.2	opt
$[Mn(CN)_4N]^-$	C_{4v}	d(Mn−N) = 1.504, d(Mn−C) = 1.967, d(C−N) = 1.165, ∠(N−Co−C) = 103.97, ∠(Mn−C−N) = 180.00	opt
$[Mn(CN)_5NO]^{2-}$	C_{4v}	d(Mn−C_{ax}) = 2.009, d(Mn−C_{eq}) = 2.025, d$(C-N)_{ax}$ = 1.167, d$(C-N)_{eq}$ = 1.168, d(Mn−N_{nitros}) = 1.722, d$(N-O)_{nitros}$ = 1.169, ∠(C_{ax}−Mn−C_{eq}) = 86.81, ∠(Mn−C−N) = 180.00	opt
$[Mn(CO)_5]$	C_{4v}	d(Mn−C_{ax}) = 1.845, d(Mn−C_{eq}) = 1.875, d$(C-O)_{ax}$ = 1.143, d$(C-O)_{eq}$ = 1.141, ∠(C_{ax}−Mn−C_{eq}) = 97.01, ∠(Mn−C_{eq}−O_{eq}) = 179.95	opt
$[Fe(CO)_5]^+$	C_{4v}	d(Fe−C_{ax}) = 1.969, d(Fe−C_{eq}) = 1.906, d$(C-O)_{ax}$ = 1.125, d$(C-O)_{eq}$ = 1.125, ∠(C_{ax}−Fe−C_{eq}) = 96.11, ∠(Fe−C_{eq}−O_{eq}) = 179.94	opt

[a] Distances in Å, angles in degrees [b] Opt = optimized in this work, otherwise the corresponding experimental reference is given. [c] Hocking, H.; Gerry, M. C.; Merrer, A. J. *Can. J. Phys.* **1979**, *57*, 54. [d] Balfour, J.; Merer, A. J.; Niki, H.; Simard, B.; Hackett, P. A. *J. Chem. Phys.* **1993**, *99*, 3288. [e] Reference 12. [f] Herzberg, H. *Spectra of Diatomic Molecules*; Van Nostrand: Princeton, New Jersey, 1950. [g] Gordon, R. M.; Merer, A. J. *Can. J. Phys.* **1980**, *58*, 642. [h] Merer, A. J. *Ann. Rev. Phys. Chem.* **1989**, *40*, 407. [i] *Landolt-Börnstein Numerical Data and Functional Relationships in Science and Technology, New Series, Group II, Vol. 21*; Madelung, O., Ed.; Springer: Berlin, 1992; p 74. [j] See text. At the DFT level, we obtain d(Cu−C) = 1.880 Å; d(C−O) = 1.140 Å. [k] Reference 53.

also to the uncertainties in the comparison between calculation and experiment.

From the solid-state EPR spectrum, only absolute values of the hyperfine tensor components (e.g., $|A_{||}|$ and $|A_{\perp}|$ for an axially symmetric center) can be determined. Additional information can be obtained, e.g., from the signs of the components of the nuclear quadrupolar tensor, so that the sign of $A_{||}$ and/or $A_{\perp}$ may be deduced.[38] Another possibility is to compare $|A_{||}|$ and $|A_{\perp}|$ from the solid-state measurement with the $|A_{iso}|$ result obtained via EPR in a solution. Unfortunately, such information is usually not available, and four combinations of A_{iso} and A_{dip} are possible. To decide which of them is the correct one, theoretical arguments have to be considered. For example, the sign of A_{dip} may be estimated from the type of the singly occupied molecular orbital (SOMO) present. Chemically similar complexes may be expected to have the same signs of $A_{||}$ and $A_{\perp}$, etc.

In this study, those signs of $A_{||}$ and $A_{\perp}$ are given in the tables (if not known experimentally), for which the resulting value of A_{dip} is as close as possible to our theoretical value. This choice is a natural one, since the calculation of the anisotropic coupling parameters is much less sensitive to the theoretical approach, and thus reasonable agreement with experiment is usually found.[13] In the majority of cases, the resulting sign turned out to be consistent with that adopted in the experimental papers. For several particular cases, the choice of sign is further discussed in the footnotes to the tables.

All values of the hyperfine parameters are given in MHz. In those cases where the experimental data have been reported in Gauss, they have been converted to MHz by multiplying with a factor of $2.80238(g/g_e)$.[2]

4. Computational Details

Molecular structures used for the hyperfine structure calculations were taken from experiment where available or have otherwise been optimized in unrestricted Kohn−Sham calculations with the B3LYP functional (using the *Gaussian 94* program[39]). The optimizations employed small-core effective-core potentials (ECPs) and (8s7p6d)/[6s5p3d] GTO valence basis sets for the metals,[40] and ECPs with (4s4p1d)/[2s2p1d] basis sets[41] for the ligand atoms (a (4s1p)/[2s1p] hydrogen basis[42] was used for MnH and $[Ni(CO)_3H]$). The resulting structure parameters are summarized in Table 1. $[Cu(CO)_3]$ is a weakly bonded complex with significant dispersion contributions to the bonding. Here the DFT optimizations are known to overestimate the Cu−C distance, and we have therefore resorted to an MP2 optimization with one f-function ($\alpha = 3.525$[43]) added to the metal basis set.

The following symmetry restrictions have been used in the optimizations: D_{3h} symmetry was used for TiF_3 and MnO_3 and for $[Cu(CO)_3]$. The trigonal planar structures are consistent with hyperfine data[44−47] and IR spectra.[48,49] D_{3h} symmetry has also been established theoretically for TiF_3 by Belanzoni et al.[17] $[Co(CO)_4]$ and $[Ni(CO)_3H]$ have C_{3v} symmetry.[50,51] T_d symmetry was used for $[Cr(CO)_4]^+$ and $[Mn(CN)_4]^{2-}$, again in agreement with experimental evidence.[52,53] C_{4v} symmetry has been imposed for $[Mn(CO)_5]$ and $[Fe(CO)_5]^+$, consistent with the EPR spectra.[54,55] DFT optimizations performed by Rosa et al.[56] for $[Mn(CO)_5]$ and by Ricca et al.[57] for $[Fe(CO)_5]^+$ have provided structural parameters close to ours. Our optimizations for $[Mn(CN)_4N]^-$, starting from the experimental C_{2v} structure of $[Mn(CN)_4N]^{2-}$,[58] converged to a regular square pyramid (C_{4v}), in agreement with the observed hyperfine structure.[58] The structure of $[Mn(CN)_5NO]^{2-}$ was optimized in C_{4v} symmetry, starting from experimental structure of Pink and Billing.[59] In discussions of the electronic structure of the complexes, we generally refer to the conventional orientation for a given point group.

The all-electron DFT calculations (cf. below for the basis sets) of the hyperfine structure were done with the *Gaussian 94* program.[39] Unless noted otherwise, unrestricted Kohn−Sham calculations were carried out. We have compared eight different combinations of exchange and correlation potentials ($\nu_x[\rho]$ and $\nu_c[\rho]$, respectively), abbreviated as BLYP, BP86, BPW91, B3LYP, B3PW91, BHLYP, BHP86, and BHPW91. The first three combine Becke's GGA functional for exchange[60] (B) with three different GGAs for correlation (LYP,[61] P86,[62] and PW91[63]). The fourth and fifth combinations use instead for exchange Becke's three-parameter hybrid functional (B3; this includes ca. 20% exact exchange).[64] Finally, for the last three functionals we have used the "half-and-half" hybrid (BH), incorporating as much as 50% exact exchange.[65] Such functionals are somewhat less popular but have been reported to perform particularly well for certain classes of open-shell main group[66] or transition metal[67] compounds. All functionals were used in their *Gaussian 94* implementation.[39] To obtain further high-level ab initio data to compare with, we have carried out coupled cluster [CCSD and CCSD(T)] calculations for a subset of molecules, using unrestricted Hartree−Fock reference wave functions (unless noted otherwise) and the ACES−II code.[68]

As a medium-size metal basis set for use in larger systems, we have constructed a (15s11p6d)/[9s7p4d] basis. Our starting point was the DZ basis of Schäfer et al.,[69] to which we added the most diffuse functions (a 1s2p1d set) from the ECP valence basis of Dolg et al.[40] IGLO−III basis sets[70] were used for the main group atoms.

Basis-set convergence was tested for several of the smaller complexes. To this end, we used a larger (21s15p10d3f)/[13s10p6d2f] metal basis, constructed from the atomic natural orbital (ANO) basis sets of Roos et al.[71] as follows: the 1s-, 2p-, 3p-, and 3d-ANO coefficients were used to contract s-functions 1−12, p-functions 1−10, p-functions 5−12, and d-functions 1−10, respectively. To this we added, in an uncontracted fashion, s-functions 10−21, p-functions 8−15, and d-functions 6−10. Finally, the 3f set of Bauschlicher et al.[72] has been added in a 21 contraction. For both the smaller and larger metal basis sets, more flexible contractions have furthermore been tested (section 5).

As a somewhat larger basis for the first-row main group atoms, we have constructed a (14s8p3d1f)/[8s6p3d1f] set, starting from the cc-pV5Z basis.[73] To the contracted sets of s-functions 1−11 and p-functions 1−8, s-functions 8−14 and p-functions 4−8 have been added in an uncontracted way, as well as three d-functions and one f-function from the cc-pVQZ basis.[73]

The results we give have been obtained with the default integration grids (int = finegrid option[39]) of the *Gaussian 94* program. For various complexes we have also tested larger angular and radial grids (results not shown). The effect of different grids was generally below 1% of the computed HFCCs, even with the largest, uncontracted basis sets.

The present calculations do not include relativistic corrections. Scalar relativistic effects on the isotropic metal HFCCs may be estimated roughly from hydrogen-like multiplicative correction factors to magnetic s-type hyperfine integrals.[74] These range from 1.036 for Sc to 1.072 for Cu. This suggests that the neglect of scalar relativistic effects may lead maximally to an underestimate of ρ_N by ca. 4−7% within the first transition metal row (in the case of a pure s-type SOMO). The influence on dipolar couplings is expected to be somewhat less pronounced. Explicit scalar relativistic DFT calculations on TiF_3[19] enhanced ρ_N(Ti) by ca. 2% and decreased A_{dip}(Ti) by a similar amount. Interestingly, these calculations indicated scalar relativistic effects for the (small) ^{19}F HFCCs on the order of ca. 10−20%. This has to be kept in mind when discussing the ligand HFCCs (section 8).

TABLE 2: Available Experimental g-Tensor Components[a]

molecule	$g_\perp$	$g_\parallel$
ScO[b]	2.0018(3)	2.0018(3)
TiF_3	1.8808	1.9902
VO[c]	1.980	2.002
$[Cr(CO)_4]^+$	1.9986	1.9986
MnH	2.001	2.0023[d]
MnO[e]	1.995	2.0023[d]
MnO_3	2.0084	2.0036
MnF	1.999	2.002[d]
MnF_2	1.999	2.002[d]
$[Mn(CN)_4]^{2-}$	2.003	2.003
$[Mn(CO)_5]$	2.043	2.004
$[Fe(CO)_5]^+$	2.0832 2.0797	2.008
$[Mn(CN)_5NO]^{2-}$	2.0311	1.9922
$[Mn(CN)_4N]^-$	2.0045	1.999
$[Co(CO)_4]$	2.1299	2.0059
$[Ni(CO)_3H]$	2.0674	2.0042
$[Cu(CO)_3]$	2.0002	2.0008

[a] See footnotes to Tables 8 and 10 for references. The g-values were usually estimated from the spectra without considering second-order effects. The g-value of the free electron is 2.0023. [b] Reference 21. [c] Reference 12. [d] Assumed in the experimental work. [e] Reference 35.

Spin−orbit effects may manifest themselves in a second-order "pseudocontact" contribution to A_{iso} ($\boldsymbol{A_{PC}}$), and in a second-order contribution to A_{dip} ($\boldsymbol{A_{dip,2}}$).[3,8,17,75] When the g-tensor of a system is known, a rough semiempirical estimate of spin−orbit contributions to the HFCCs may be obtained along the lines of the classical perturbation theoretical approach of Abragam and Pryce[76] (more details for specific d-orbital occupations and coordination arrangements are given in ref 8). For example, for a d^1-system in a trigonally distorted octahedral field (d_{z^2}-configuration), we may use equations (9.204)−(9.209) in ref 8 to get

$$A_\parallel = A_{FC} + P\left[\frac{4}{7}\delta^2 - \frac{1}{7}\Delta g_\perp\right]$$

$$A_\perp = A_{FC} + P\left[-\frac{2}{7}\delta^2 + \frac{15}{14}\Delta g_\perp\right] \qquad (4)$$

where $P = (\mu_0/4\pi)2\mu_B\langle r^3\rangle$, δ is d_{z^2}-orbital coefficient in the SOMO, and $\Delta g_\perp = g_e - g_\perp$. Now, setting $(2/7)\delta^2 P = A_{dip}$, we get

$$A'_\parallel = A_\parallel - A_{FC} = A_{dip}\left[2 - \frac{\Delta g_\perp}{2\delta^2}\right]$$

$$A'_\perp = A_\perp - A_{FC} = A_{dip}\left[-1 + \frac{15\Delta g_\perp}{4\delta^2}\right] \qquad (5)$$

Since $A'_\perp = -A_{dip} - A_{dip,2} + A_{PC}$ and $A_{PC} = {}^1/_3(A'_\parallel + 2A'_\perp)$, we get

$$A_{PC} = \frac{7}{3}\frac{\Delta g_\perp A_{dip}}{\delta^2} \qquad A_{dip,2} = -\frac{17}{12}\frac{\Delta g_\perp A_{dip}}{\delta^2} \qquad (6)$$

Using our DFT results for A_{dip} (we chose the BPW91 data), together with experimental values of the g-tensor components (Table 2), we may thus approximately estimate the spin−orbit

TABLE 3: Coupled-Cluster Results (in MHz)

	9s7p4d			15s10p6d2f		
molecule	RCCSD	UCCSD	UCCSD(T)	UCCSD	UCCSD(T)	exp[a]
A_{iso}(M)						
^{2}ScO		1823.1	1819.2	1837.3	1837.1	1947.339(2)
^{4}VO		676.6	730.4	702.1	740.8	778(2)
^{6}MnO	416.6	441.6	435.2	467.6	460.6	479.9
^{6}MnF$_2$	64.4	63.0	77.3			104(6)[b]
^{7}MnH		217.0	216.7	242.2	243.4	279.4
^{2}TiF$_3$	−170.9	−170.5				−177.1(4)[b]
^{2}MnO$_3$	1492.0	1511.3				1613(6)
^{2}CuO		−498.9	−515.0	−538.4	−552.1	−483.6(94)
A_{dip}(M)						
^{2}ScO		23.1	23.9	23.7	24.3	24.8
^{4}VO		−46.5	−46.3	−47.6	−46.5	−41.2
^{6}MnO	−16.0	−16.7	−17.3	−16.9	−17.8	−16.1
^{6}MnF$_2$	4.2	4.1	3.5			10(6)[b]
^{7}MnH		12.0	12.0	12.6	12.6	12.0(8)
^{2}TiF$_3$	−7.5	−7.5				−6.6(4)[b]
^{2}MnO$_3$	94.7	101.5				81(3)
^{2}CuO		34.4	34.9	44.6	46.2	24.1
A_{iso}(X)						
^{2}ScO		−17.4	−23.9	−17.3	−23.7	−20.3(3)[b]
^{4}VO		3.8	3.8	4.2	3.4	0(4)
^{6}MnO	−5.1	−7.0	−6.9	−8.2	−7.9	
^{6}MnF$_2$	9.9	9.9	9.5			
^{7}MnH		13.6	13.8	15.3	17.1	20.7(39)
^{2}TiF$_3$	−33.3	−35.1				8.3(4)[c]
^{2}MnO$_3$	4.9	7.8				
^{2}CuO		−42.7	−40.9	−43.6	−41.6	
A_{dip}(X)						
^{2}ScO		0.4	−0.1	0.7	−0.1	0.4(2)[b]
^{4}VO		2.2	−3.2	1.4	−2.7	0(3)
^{6}MnO	9.2	11.1	8.6	11.5	8.7	
^{6}MnF$_2$	−10.3	−10.2	−10.6			
^{7}MnH		11.8	11.8	11.9	11.8	8.4(33)
^{2}TiF$_3$[d]	18.0, 6.1, −24.0	18.7, 5.9, −24.6				*e*
^{2}MnO$_3$[d]	−22.6, −7.7, 30.3	−27.0, −35.8,62.8				
^{2}CuO		57.6	55.9	57.6	55.8	
	$\langle S^2\rangle_{CC}/\langle S^2\rangle_{UHF}$					nominal $\langle S^2\rangle$
^{2}ScO		0.751/0.756	0.750/0.756	0.751/0.755	0.750/0.755	0.750
^{4}VO		3.779/4.229	3.741/4.229	3.782/4.238	3.739/4.238	3.750
^{6}MnO	8.838/8.750	8.828/9.534	8.727/9.534	8.859/9.532	8.722/9.532	8.750
^{6}MnF$_2$	8.752/8.750	8.762/8.752	8.750/8.762			8.750
^{7}MnH		12.000/12.005	12.000/12.005	12.001/12.005	12.000/12.005	12.000
^{2}TiF$_3$	0.750/0.750	0.750/0.753				0.750
^{2}MnO$_3$	0.771/0.750	1.068/2.601				0.750
^{2}CuO		0.754/0.772	0.750/0.772	0.754/0.772	0.750/0.772	0.750

[a] Cf. footnotes to Tables 8 and 10 for sources of experimental data. [b] Ne matrix result. Tables 8−11 also include the Ar matrix results. [c] Reference 44, cf. reference 18 for a revision. [d] Nonaxial tensor. The T_{ii} components are given in order: (1) along the metal−ligand bond, (2) normal to the metal−ligand bond, in the molecular plane, (3) along the molecular *z*-axis. [e] Anisotropy experimentally not well defined, cf. discussion in reference 18.

contributions to the hyperfine parameters from eq 6. The values of δ were obtained from the Mulliken population analysis of the SOMO composition. The formulas given here may be used for any axially symmetric system with the SOMO dominated by the metal d_{z^2} orbital. This approach is used for TiF$_3$, [Mn(CO)$_5$], [Fe(CO)$_5$]$^+$, [Ni(CO)$_3$H], and [Co(CO)$_4$]. We use related formulae to estimate the spin−orbit contributions for [Mn(CN)$_5$NO]$^{2-}$, where the SOMO is a metal d_{xy} orbital. In essentially all other cases, deviations of the g-tensors from the free-electron g-value are sufficiently small to expect negligible spin−orbit effects on the HFCCs (no experimental g-tensor is available for CuO; for this complex we expect significant SO effects, cf. section 7). We should also note that the assumption of the d_{z^2} orbital dominating the SOMO is not entirely appropriate for [Mn(CO)$_5$] and [Ni(CO)$_3$H] (significant 4p$_z$ character has to be considered), which may lead to a significant error in the estimate (see section 7).

5. Coupled-Cluster Results

The CCSD and CCSD(T) calculations carried out on a subset of complexes (ScO, VO, MnO, MnF$_2$, MnH, TiF$_3$, MnO$_3$, and CuO) should provide benchmark data for the validation of the more economical DFT approaches. The results are summarized in Table 3. Both the standard 9s7p4d and the more flexible 15s10p6d2f metal basis sets were used for the diatomics (see also section 6), together with the IGLO−III basis for the ligand atoms. With the available computational resources we could not use the larger basis set for MnF$_2$, TiF$_3$, or MnO$_3$ (for the latter two complexes, even the CCSD(T) calculations with the smaller basis exceeded our available resources). While the larger basis should be essentially saturated in the important range of the outermost core shells (cf. section 6), it is probably still incomplete with respect to higher angular-momentum functions necessary for the explicit description of electron correlation.

Disregarding CuO for the moment, the results of the largest CCSD(T)/15s10p6d2f calculations for the isotropic metal coupling constants are only ca. 4−5% below experiment. For the smaller absolute value in MnH, the deviation is ca. 13% (again the computational result is too low). A similar underestimation of the experimental metal HFCCs was also found in the few available previous post-Hartree−Fock studies.[9−12] These results suggest that the coupled-cluster calculations underestimate electron correlation, mainly because of basis-set incompleteness, and therefore may overestimate spin polarization to some extent. Of course we have to remember that scalar relativistic effects and rovibrational corrections have not been considered (cf. section 4). CuO differs from the other cases, as both basis-set extension and inclusion of triple excitations leads to more negative A_{iso}(Cu) and thus to inferior agreement with experiment (although still better than with DFT methods, see below). The discrepancy is probably related to the neglect of spin−orbit corrections (see discussion in section 7).

Comparison of CCSD(T) and CCSD results indicates that the perturbative inclusion of triple excitations is particularly notable for MnF_2 and VO, where the positive triples contribution brings the results closer to experiment (note that for VO the triples contribution is less pronounced with the larger basis set). In all other cases, the influence of triple excitations is small. We note that the inclusion of triple excitations brings our CCSD(T) data for VO into better agreement with experiment than the SDCI and MRCI results of Knight et al. (ca. 685−692 MHz with different basis sets, which are comparable to the ones used here).[12]

Use of the smaller 9s7p4d metal basis leads to a reduction of A_{iso}(M) by ca. 9% for MnH, by ca. 5% for MnO, by ca. 3% for CuO, and by only ca. 1% for VO and ScO. While this is in part due to some error compensation, it indicates already that the 9s7p4d basis provides a good compromise between computational effort and accuracy. This is confirmed in the DFT calculations (see below). We expect that a larger basis should bring the result for MnF_2 closer to the Ne matrix value. The CCSD results for TiF_3 and MnO_3 with the 9s7p4d metal basis are already in good agreement with experiment (cf. Table 3). Even for the latter system, the coupled cluster wave function corrects quite efficiently the significant spin contamination of the UHF reference (cf. $<S^2>$ values in Table 3; this behavior of the CC approach was discussed before[77,78]). Despite the remaining contamination, the RCCSD and UCCSD results for $A_{iso}(Mn)$ are already quite close. Differences are still apparent for A_{dip}(Mn) and for the ligand HFCCs. Spin contamination of the UHF reference wave function for MnO and MnF_2 is lower, and thus the agreement between RCCSD and UCCSD results is even closer. This indicates the relative stability of the CC approach with respect to the quality of the reference wave function.[77,78] A more detailed analysis of different reference wave functions is beyond the scope of the present study.

The small dipolar coupling constants for the metals are reproduced rather accurately for most systems. The less favorable agreement for MnF_2 might be due to matrix effects (cf. Table 8), whereas the description of CuO is generally more complicated, probably due to spin−orbit effects (cf. above and section 7). Except for the latter complex, the dependence of A_{dip}(M) on triple excitations and basis set is only moderate, as one might expect. Agreement of the CC results with available experimental ligand isotropic and anisotropic HFCCs may also be considered reasonable in most cases, in view of their smallness in absolute terms (note the significant error bar on the experimental result for VO).

TABLE 4: Basis-Set Dependence of the HFCC (MHz) in Mn^+ [a]

basis	A_{iso}(Mn)
(15s11p6d)/[9s7p4d][b]	759.2
9s7p4d + 1s[c]	757.0
9s7p4d + 2s[c]	744.8
9s7p4d + 3s[c]	729.5
15s11p6d uncontr.[d]	728.4
(21s15p10d3f)/[13s10p6d2f]	841.9
13s15p6d2f (all p-orb. uncontr.)	841.9
13s10p10d2f (all d-orb. uncontr.)	840.8
13s10p6d2f + 1s[c]	811.0
13s10p6d2f + 2s[c]	802.6
13s10p6d2f + 3s[c]	798.5
13s10p6d2f + 4s[c]	798.3
13s10p6d2f + 5s[c]	797.6
21s10p6d2f (all s-orb. uncontr.)	797.8
21s15p10d3f uncontr.[d]	797.4
exp[f]	757.8[e]

[a] B3PW91 results. [b] Standard 9s7p4d basis. [c] Outermost core s-functions added in an uncontracted way, see text. [d] Fully uncontracted. [e] All s-functions uncontracted. Kasai, P. H. *Acc. Chem. Res.* **1971**, *4*, 329. Ar-matrix isolation. [f] Reference 45 reports a value of 771(14) MHz.

6. Basis-Set Study

While the basis-set dependence of the hyperfine parameters for light main group atoms and molecules has already been investigated in detail,[13,15,79,80] systematic basis-set studies are lacking for transition metal systems, except for a comparison of different STO basis-sets for TiF_3 by Belanzoni et al.[17] For several small systems, we have therefore studied the GTO basis-set convergence at the DFT level.

Table 4 examines the B3PW91 results for A_{iso} in the $^7Mn^+$ cation, using a variety of basis sets. For this high-spin cation with d^5s^1 configuration, the large positive direct contribution to the HFCC due to the single s-type SOMO should be partially compensated by negative contributions from spin polarization of the core shells, due to the five d-type SOMOs.[81] A better description of this spin polarization should thus reduce the HFCC. From tests with still larger basis sets, we expect the fully uncontracted 21s15p10d3f basis to be converged to within better than ca. 10 MHz. Comparison of the resulting 797 MHz to the 980 MHz obtained at the restricted B3PW91 level (with the same basis) suggests a total spin-polarization contribution of ca. −183 MHz. Remaining differences to experiment (note the two different experimental values available in the literature; footnotes e,f to Table 4) are expected to be largely the result of deficiencies in the exchange−correlation potential,ν_{xc}. Contraction of the basis to 13s10p6d2f increases the HFCC by ca. 43 MHz. Starting from this contraction, we may now examine the influence of partial decontraction. Changes in the p- and d-basis have negligible effects. However, if we add s-function 9 (α = 316.3768) in an uncontracted fashion, 30 MHz of the 43 MHz contraction error have been eliminated. Adding s-exponents 8 (α = 727.3039) and 7 (α = 1755.212) reduces the HFCC by another 8 and 4 MHz, respectively, giving 798.5 MHz for the resulting 15s10p6d2f basis, i.e., almost the value obtained with the fully uncontracted basis (further addition of uncontracted tighter s-functions has thus very little effect). Our MO analyses indicate that this is mainly due to a decrease in the direct SOMO contribution, possibly due to a better description of the nodal structure of the 4s-orbital.

We may also analyze the results obtained with our smaller 9s7p4d standard basis constructed for use in larger systems. Employing this basis fully uncontracted to 15s11p6d, the expected basis-set limit HFCC (for the B3PW91 functional used)

TABLE 5: Basis-Set Dependence of Hyperfine Parameters (in MHz) in MnO[a]

basis set		BP86				B3LYP				B3PW91			
Mn	O	A_{iso}(Mn)	A_{dip}(Mn)	A_{iso}(O)	A_{dip}(O)	A_{iso}(Mn)	A_{dip}(Mn)	A_{iso}(O)	A_{dip}(O)	A_{iso}(Mn)	A_{dip}(Mn)	A_{iso}(O)	A_{dip}(O)
9s7p4d[b]	IGLO−III	526.8	−24.4	−5.4	8.1	521.8	−20.7	−8.0	9.9	507.5	−20.2	−7.3	10.1
9s7p4d +3s[c]	IGLO−III	507.3	−24.5	−5.4	8.1	502.5	−20.7	−8.0	9.9	485.9	−20.3	−7.6	9.9
15s11p6d (uncontr.[d])	IGLO−III (uncontr.[d])	507.1	−24.9	−5.3	8.1	501.9	−21.1	−7.9	9.9	488.2	−20.6	−7.2	10.1
13s10p6d2f[e]	8s6p3d1f[f]	562.5	−24.2	−5.5	8.3	557.7	−20.4	−8.0	10.0	543.3	−20.0	−7.8	10.3
13s10p6d2f +2s[g]	8s6p3d1f[f]	539.9	−24.2	−5.4	8.3	534.8	−20.4	−7.7	10.2	518.2	−20.0	−7.4	10.3
13s10p6d2f +2s[g]	IGLO−III	534.5	−24.2	−5.3	8.3	532.9	−20.4	−7.5	10.2	516.3	−20.0	−7.2	10.3
21s15p10d3f (uncontr.[d])	8s6p3d1f (uncontr.[d])	531.5	−24.6	−5.4	8.4	527.5	−20.5	−8.0	10.0	513.7	−20.1	−7.3	10.3

[a] Experimental data: A_{iso}(Mn) = 479.861(100) MHz, A_{dip}(Mn) = −16.066(59) MHz (gas-phase measurement, ref 36). [b] (15s11p6d)/[9s7p4d]. [c] Three outermost core s-functions added, see text. [d] Fully uncontracted. [e] (21s15p10d3f)/[13s10p6d2f]. [f] Larger ligand basis, see Computational Methods. [g] Two outermost core s-functions added, see text.

TABLE 6: Dependence of Metal HFCCs (in MHz) on the Metal Basis-Set for Selected Systems[a]

		BP86			B3LYP			B3PW91			
molecule		9s7p4d	12s7p4d[b]	15s10p6d2f[c]	9s7p4d	12s7p4d[b]	15s10p6d2f[c]	9s7p4d	12s7p4d[b]	15s10p6d2f[c]	exp[d]
^{2}ScO	A_{iso}	1979.6	1898.4	1932.0	2032.3	1948.2	1995.6	1930.2	1849.9	1878.6	1947.339(2)
	A_{dip}	17.5	17.5	18.8	18.7	18.7	20.1	18.7	18.7	20.1	24.8053(7)
^{2}TiN	A_{iso}	−569.0	−547.3	−561.8	−584.3	−559.7	−578.1	−554.2	−534.1	−548.1	−558.8(11)
	A_{dip}	−4.3	−4.3	−4.7	−4.4	−4.5	−4.9	−4.7	−4.6	−5.1	−5(2)
^{4}VO	A_{iso}	821.0	789.8	815.4	829.5	796.5	825.5	795.2	763.0	788.8	778(2)
	A_{dip}	−48.1	−48.0	−48.1	−49.9	−49.8	−50.0	−48.2	−48.2	−48.1	−41.3(8)
^{6}MnO	A_{iso}	526.8	507.3	534.5	521.8	502.5	532.9	507.5	485.9	516.3	479.861(100)
	A_{dip}	−24.4	−24.5	−24.2	−20.7	−20.7	−20.4	−20.2	−20.3	−20.0	−16.066(59)
^{7}MnH	A_{iso}	380.0	366.7	398.1	331.8	322.1	349.0	329.6	322.3	351.7	279.4(12)
	A_{dip}	8.4	8.3	9.0	9.8	9.7	10.4	10.1	10.1	10.9	12.0(8)

[a] The IGLO-III basis was used for the ligands. [b] Three outermost core functions added to standard 9s7p4d basis, see text. [c] Two outermost core functions added to 13s10p6d2f basis, see text. [d] See footnotes to Tables 8 and 10 for the sources of experimental data.

is underestimated by ca. 70 MHz (Table 4). This is most probably related to the lack of very large core−shell s-exponents to describe accurately the spin density near the nucleus. Upon contraction, the discrepancy with respect to the 21s15p10d3f basis result decreases, again due to an increased SOMO contribution. The medium-size 9s7p4d basis simulates the largest basis sets quite well, due to error compensation. We find this compensation to be systematic rather than accidental (see below) and take it as a support for the usefulness of this smaller metal basis for applications to larger systems.

Table 5 shows basis-set tests for both metal and ligand isotropic and dipolar HFCCs in MnO, using three different functionals. First of all, we note that the anisotropies show relatively little basis-set dependence. Examination of the effect of the ligand basis set on the isotropic HFCCs indicates that the IGLO−III basis is already rather well converged relative to the larger 8s6p3d1f basis. The effect of the metal basis is very similar to the above results for Mn^+. Decontraction of the outermost core−shell s-functions decreases A_{iso}(Mn). The smaller 9s7p4d basis compares again well with the fully uncontracted 21s15p10d3f basis (for all functionals), due to error compensation.

Table 6 shows results for A_{iso}(M) and A_{dip}(M) of a somewhat larger subset of molecules with three different basis sets (9s7p4d, 9s7p4d+3s, 13s10p6d2f+2s), and again with three functionals. As in the two previous cases, a more flexible description of the outermost s-core shell regions (2s, 3s) reduces the absolute value of A_{iso}(M) (TiN has a negative HFCC due to the negative g_N(Ti); cf. Table 7). Notably, the contracted 9s7p4d basis gives results that deviate only by ca. 1−2% from the values obtained with the flexible 15s10p6d2f basis. Only for MnH, the deviation is ca. 5%. This gives further justification to our use of the 9s7p4d basis as the standard metal basis set for the remainder of this study.

TABLE 7: Nuclear g-Values[a]

isotope	g-value
^{45}Sc	1.35883
^{47}Ti	−0.31538
^{51}V	1.47100
^{53}Cr	−0.31567
^{55}Mn	1.37960
^{57}Fe	0.18084
^{59}Co	1.31886
^{61}Ni	−0.49987
^{63}Cu	1.48187
^{1}H	5.58556
^{13}C	1.40480
^{14}N	0.40375
^{17}O	−0.75748
^{19}F	5.25760

[a] In nuclear magnetons. Taken from Fuller, G. H. *J. Chem. Phys. Ref. Data* **1976**, *5*, 835.

7. Performance of Different Exchange−Correlation Functionals for Metal HFCCs

General Trends. We will start by discussing some general trends before going into more detailed analyses for specific groups of complexes. Table 8 gives isotropic metal HFCCs, Table 9 the dipolar couplings for all 21 molecules and for the eight functionals of this study, in comparison with experiment. The dipolar couplings give us further insight, as they depend less on subtle details of spin polarization but more on the overall quality of our wave functions. Additional insight on spin contamination is provided by the $<S^2>$ expectation values, which are also included in Table 9.[82]

Figures 1−7 show graphically for groups of related complexes the spin-density at the metal nuclei, and for all functionals, normalized to the number of unpaired electrons. Two general trends hold with very few exceptions: (i) For a given exchange

TABLE 8: Dependence of Isotropic Metal HFCCs on the Exchange−Correlation Functional (in MHz)

	BLYP	BP86	BPW91	B3LYP	B3PW91	BHLYP	BHP86	BHPW91	exp[a]
^{2}ScO	2043.5	1979.6	1933.5	2032.3	1930.2	1904.7	1983.1	1847.7	1947.339(2)[b,c]
^{2}TiN	−587.0	−569.0	−556.6	−584.3	−554.2	−569.6	−540.7	−528.0	−558.8(11)[b,d]
^{3}TiO	−257.5	−251.0	−246.3	−252.8	−242.4	−241.9	−233.2	−227.0	−241.0 (60)[b,d]
^{3}VN	1432.6	1393.5	1357.8	1388.9	1315.4	1168.9	1124.6	1081.7	1311.8[b,e]
^{4}VO	847.8	821.0	811.9	829.5	795.2	795.0	763.3	753.4	778(2)[b,f]
^{6}MnO	543.1	526.8	524.0	521.8	507.5	528.5	509.8	504.7	479.861(100)[b,g]
^{6}MnF$_2$	313.0	294.2	283.9	240.7	214.1	144.9	118.5	109.0	104(6), 134(6)[h,i]
^{7}MnF	501.9	480.6	473.9	470.5	443.6	422.3	397.4	391.5	442(6), 443(6)[h,i]
^{7}MnH	380.0	380.0	385.0	331.8	329.6	277.1	271.8	276.3	279.4(12)[b,j]
^{2}TiF$_3$	−218.0	−216.6	−211.6	−192.2	−186.1	−157.8	−151.9	−149.4	−184.8(4), −177.1(4)[h,k]
^{2}MnO$_3$	2042.4	2009.3	1987.2	1735.5	1675.9	1187.6	1141.5	1111.7	1613(6)[h,l]
^{6}[Mn(CN)$_4$]$^{2-}$	−90.8	−99.8	−104.8	−116.6	−132.0	−155.0	−169.3	−176.0	−199(3)[m]
^{6}[Cr(CO)$_4$]$^+$	21.9	23.8	25.2	26.9	30.8	34.5	38.4	40.4	41.5[n,o]
^{2}[Mn(CO)$_5$]	6.7	2.8	0.8	−2.5	−12.1	−21.4	−32.0	−37.6	−2.8, 0.6, 5.6[p]
^{2}[Fe(CO)$_5$]$^+$	1.1	0.0	−0.6	−3.2	−5.3	−9.3	−11.7	−12.3	−2.2[q]
^{2}[Mn(CN)$_5$NO]$^{2-}$	−134.3	−145.8	−153.8	−223.6	−259.2	−304.5	−351.7	−364.1	−219.5[r]
^{2}[Mn(CN)$_4$N]$^-$	−160.1	−170.4	−176.0	−250.1	−275.0	−506.7	−548.5	−558.5	−276[s]
^{2}[Ni(CO)$_3$H]	24.4	22.3	23.5	33.3	33.9	51.3	54.8	56.0	9.0(2)[n,t]
^{2}[Co(CO)$_4$]	−6.4	−11.3	−15.7	−61.4	−75.4	−175.4	−210.0	−219.7	−47.8, −52(1)[u]
^{2}CuO	−651.8	−640.0	−678.1	−755.2	−776.4	−732.4	−676.4	−717.3	−483.6(94)[b,v]
^{2}[Cu(CO)$_3$]	−19.2	−7.3	−7.1	4.7	13.0	45.0	68.8	67.9	71.2[w]

[a] The numbers in parentheses represent standard deviations. [b] Gas-phase measurement. [c] Reference 28. [d] Reference 29. For the TiO molecule, parameter "*c*" determining the dipolar contribution has not been resolved. Our B3PW91/9s7p4d result for $A_{dip}(= c/3)$ has been used to derive $A_{iso}(= b + c/3)$ from the reported sum $b + c = -231.6(60)$ MHz. [e] Balfour, J.; Merer, A. J.; Niki, H.; Simard, B.; Hackett, P. A. *J. Chem. Phys.* **1993**, *99*, 3288. Our B3PW91/9s7p4d result for $A_{dip}(= c/3)$ has been used to derive $A_{iso}(=b + c/3)$ from the reported sum $b + c = 1264.2$ MHz. [f] Reference 33. [g] Reference 36. See also references given therein. [h] EPR in Ne and Ar matrix, respectively. [i] DeVore, C.; Van Zee, J. R.; Weltner, W. Jr. *J. Chem. Phys.* **1978**, *68*, 3522. [j] Reference 37. [k] Reference 44. [l] Reference 45. [m] EPR in solution, ref 53. [n] EPR in Kr matrix. [o] Reference 52. [p] (1)EPR in Ar matrix, ref 54. (2) Solid-state EPR: Ozin, G. A., personal communication cited by Huffadine, A. S.; Peake, B. M.; Robinson B. M.; Simpson, J; Davson, P. A. *J. Organomet. Chem.* **1976**, *121*, 391. (3) EPR in C_6D_6 matrix: Howard, J. A.; Morton, J. R.; Preston, K, F. *Chem. Phys. Lett.* **1982**, *83*, 1226. [q] EPR in $Cr(CO)_6$ host crystal, ref 55. [r] Single-crystal EPR in a host lattice of $Na_2Fe(CN)_5NO{\cdot}2H_2O$: Manoharan, T.; Gray, H. B. *Inorg. Chem.* **1966**, *5*, 823. [s] EPR in CH_3CN at 300 and 10 K, cf. ref 58. Relative signs are known. [t] Reference 51. The sign of the $A_{\|}(+)$ has been determined from the sign of the nuclear quadrupolar coupling tensor component. [u] EPR in solid Kr, ref 50; EPR in CO matrix, cf. ref 88b. [v] Steimle, T.; Namiki, K.; Saito, S. *J. Chem. Phys.* **1997**, *107*, 6109. [w] EPR in Ar matrix, refs 46 and 47.

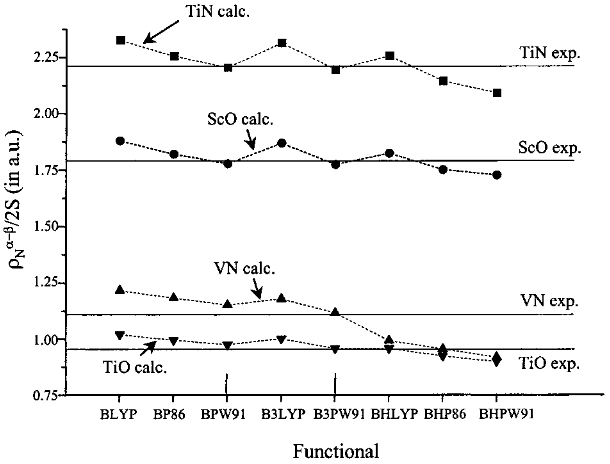

Figure 1. Spin density $\rho_N^{\alpha-\beta}$ at the metal nuclei in ^{2}ScO, ^{3}TiO, ^{2}TiN, and ^{3}VN, normalized to the number of unpaired electrons. Dependence on ν_{xc}.

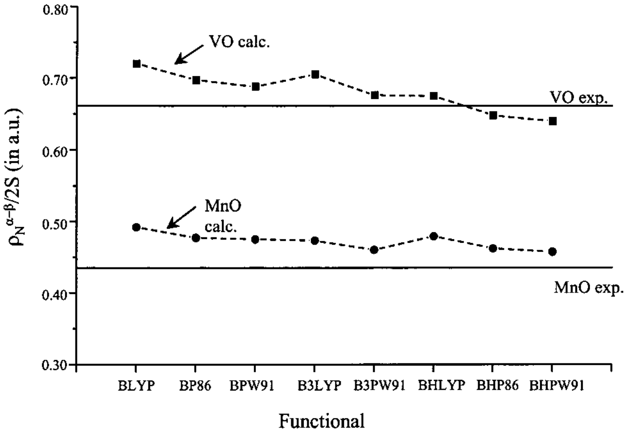

Figure 2. Spin density $\rho_N^{\alpha-\beta}$ at the metal nuclei in ^{4}VO and ^{6}MnO, normalized to the number of unpaired electrons. Dependence on ν_{xc}.

functional $\nu_x[\rho]$, the computed spin density ρ_N at the metal nucleus depends on the correlation functional $\nu_c[\rho]$ as ρ_N(LYP) $\geq \rho_N$(P86) $\geq \rho_N$(PW91). (ii) For a given correlation functional, ρ_N decreases such as $\rho_N(B) \geq \rho_N(B3) \geq \rho_N(BH)$, i.e., the spin density is reduced with increasing admixture of exact exchange. The latter trend is consistent with the expectation that the "pure" GGA functionals underestimate spin polarization.[13,14,83,84] As the core−shell contributions to this spin polarization dominate typically in transition metals and contribute overall negatively to ρ_N (see above), the metal HFCCs tend to be overestimated at the GGA level. It is well known that unrestricted Hartree−Fock wave functions tend to overestimate spin polarization (accompanied by spin contamination). Therefore, the inclusion of exact exchange into $\nu_x[\rho]$ is expected to increase spin polarization and thus to decrease A_{iso}(M).

The relative sensitivity of the results to $\nu_x[\rho]$ and $\nu_c[\rho]$ depends strongly on the particular system. For ScO, TiN, or TiO, a change in ν_c (e.g. BLYP → BP86 → BPW91) influences the results considerably more than the change of ν_x from B to B3 (Figure 1). For TiF_3, MnH or MnF_2, and for several other complexes, the behavior is just the opposite, i.e., the dependence on ν_x dominates (e.g., Figures 3 and 4). In other cases, the dependence on ν_x and ν_c is of comparable magnitude (see, e.g., Figure 2). Except for cases with strong spin contamination (cf. below), the effects of ν_x and ν_c appear to be roughly additive.

The overall range of variation of the HFCCs for different functionals is also rather diverse in different systems. Thus, for some systems the range of results encompasses only some

TABLE 9: Dependence of Dipolar Metal HFCCs on the Exchange−Correlation Functional (in MHz)

molecule		BLYP	BP86	BPW91	B3LYP	B3PW91	BHLYP	BHP86	BHPW91	exp.[a] *nominal* $\langle S^2\rangle$
^{2}ScO	A_{dip}	17.1	17.5	17.3	18.7	18.7	21.1	21.2	21.0	24.8053(7)
	$<S^2>$	*0.751*	*0.752*	*0.752*	*0.751*	*0.752*	*0.751*	*0.752*	*0.753*	*0.750*
^{2}TiN	A_{dip}	−4.1	−4.3	−4.3	−4.4	−4.7	−5.0	−5.2	−5.3	−5(2)
	$<S^2>$	*0.752*	*0.754*	*0.756*	*0.753*	*0.759*	*0.757*	*0.768*	*0.769*	*0.750*
^{3}TiO	A_{dip}	−5.0	−4.7	−4.7	−5.0	−4.7	−5.1	−4.9	−4.9	
	$<S^2>$	*2.009*	*2.011*	*2.014*	*2.012*	*2.017*	*2.016*	*2.020*	*2.024*	*2.000*
^{3}VN	A_{dip}	−29.7	−28.0	−26.6	−26.3	−23.8	−16.0	−14.8	−14.0	
	$<S^2>$	*2.034*	*2.040*	*2.047*	*2.076*	*2.119*	*2.424*	*2.442*	*2.505*	*2.000*
^{4}VO	A_{dip}	−49.8	−48.1	−47.7	−49.9	−48.2	−50.9	−49.9	−48.9	−41.3(8)
	$<S^2>$	*3.784*	*3.791*	*3.798*	*3.799*	*3.815*	*3.817*	*3.817*	*3.841*	*3.750*
^{6}MnO	A_{dip}	−24.9	−24.4	−24.3	−20.7	−20.2	−16.2	−16.2	−16.0	−16.066(59)
	$<S^2>$	*8.783*	*8.788*	*8.794*	*8.827*	*8.848*	*9.034*	*9.059*	*9.078*	*8.750*
^{6}MnF$_2$	A_{dip}	−7.8	−6.4	−6.4	−3.6	−2.2	0.8	2.0	2.2	10(6) or 6(6)[b]
	$<S^2>$	*8.758*	*8.760*	*8.761*	*8.760*	*8.762*	*8.760*	*8.761*	*8.762*	*8.750*
^{7}MnF	A_{dip}	5.6	6.2	6.2	7.0	7.6	8.4	8.7	8.7	24(6), 16(6)
	$<S^2>$	*12.002*	*12.003*	*12.003*	*12.003*	*12.003*	*12.003*	*12.003*	*12.003*	*12.000*
^{7}MnH	A_{dip}	7.8	8.4	8.4	9.8	10.1	10.9	11.2	11.2	12.0(8)
	$<S^2>$	*12.003*	*12.004*	*12.004*	*12.003*	*12.004*	*12.002*	*12.003*	*12.004*	*12.000*
^{2}TiF$_3$	A_{dip}	−9.9	−9.2	−9.1	−10.1	−9.5	−9.9	−9.5	−9.3	−6.6(4), −8.1(4)[b]
	$<S^2>$	*0.752*	*0.752*	*0.753*	*0.752*	*0.753*	*0.752*	*0.752*	*0.753*	*0.750*
^{2}MnO$_3$	A_{dip}	95.9	95.1	95.5	124.5	125.9	178.0	174.2	171.4	81(3)
	$<S^2>$	*0.765*	*0.768*	*0.770*	*0.880*	*0.914*	*2.0025*	*1.994*	*2.054*	*0.750*
^{6}[Mn(CN)$_4$]$^{2-}$	A_{dip}	0.0	0.0	0.0	0.0	0.0	0.0	0.0	0.0	0[c]
	$<S^2>$	*8.762*	*8.764*	*8.765*	*8.762*	*8.766*	*8.763*	*8.765*	*8.766*	*8.750*
^{6}[Cr(CO)$_4$]$^+$	A_{dip}	0.0	0.0	0.0	0.0	0.0	0.0	0.0	0.0	0.0
	$<S^2>$	*8.757*	*8.761*	*8.762*	*8.759*	*8.764*	*8.761*	*8.765*	*8.765*	*8.750*
^{2}[Mn(CO)$_5$]	A_{dip}	97.0	96.1	96.2	96.5	95.8	88.6	88.4	89.0	90(8) − 92(6)[d]
	$<S^2>$	*0.753*	*0.753*	*0.754*	*0.758*	*0.759*	*0.773*	*0.773*	*0.776*	*0.750*
^{2}[Fe(CO)$_5$]$^+$	A_{dip}	18.5	18.3	18.2	19.3	19.0	19.7	19.5	19.6	15.4
	$<S^2>$	*0.757*	*0.757*	*0.756*	*0.763*	*0.764*	*0.770*	*0.770*	*0.771*	*0.750*
^{2}[Mn(CN)$_5$NO]$^{2-}$	A_{dip}	−97.3	−98.2	−96.2	−58.1	−56.0	−30.3	−30.2	−29.0	−115.2
	$<S^2>$	*0.868*	*0.850*	*0.866*	*1.440*	*1.464*	*2.091*	*2.077*	*2.086*	*0.750*
^{2}[Mn(CN)$_4$N]$^-$	A_{dip}	−116.2	−115.2	−115.1	−117.2	−115.6	−88.5	−88.7	−89.2	−122.4
	$<S^2>$	*0.774*	*0.773*	*0.775*	*0.882*	*0.896*	*1.763*	*1.784*	*1.796*	*0.750*
^{2}[Ni(CO)$_3$H]	A_{dip}	−49.8	−49.6	−49.6	−56.9	−56.5	−67.8	−67.2	−66.8	−44.0(2)
	$<S^2>$	0.752	0.752	0.752	0.757	0.756	0.793	0.791	0.793	0.750
^{2}[Co(CO)$_4$]	A_{dip}	153.6	152.4	151.8	147.4	146.2	101.2	93.6	84.5	110.0
	$<S^2>$	*0.762*	*0.761*	*0.763*	*0.788*	*0.789*	*0.930*	*0.957*	*1.005*	*0.750*
^{2}CuO	A_{dip}	42.7	41.6	41.8	33.7	33.4	22.8	20.8	21.6	24.1
	$<S^2>$	*0.762*	*0.761*	*0.762*	*0.767*	*0.768*	*0.768*	*0.765*	*0.767*	*0.750*
^{2}[Cu(CO)$_3$]	A_{dip}	65.2	65.7	64.8	65.9	65.4	58.4	58.8	58.3	81
	$<S^2>$	*0.751*	*0.752*	*0.752*	*0.753*	*0.754*	*0.756*	*0.757*	*0.758*	*0.750*

[a] See corresponding footnotes to Table 8 for the sources of the experimental data. [b] EPR in Ne and Ar matrix, respectively. [c] Not observed (zero due to symmetry). [d] EPR using different solid matrices.

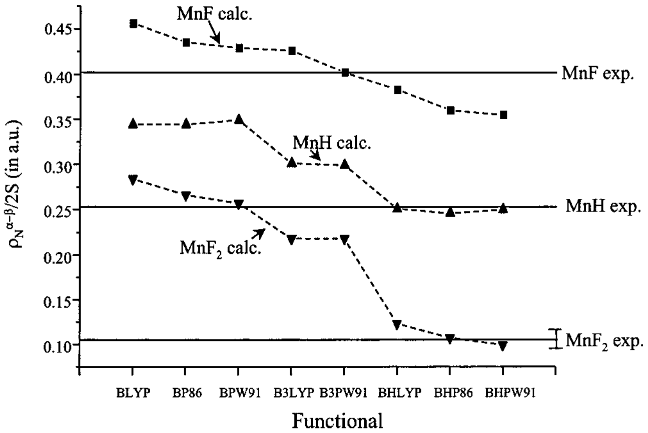

Figure 3. Spin density $\rho_N^{\alpha-\beta}$ at the metal nuclei in $^2TiF_3$ and $^2MnO_3$, normalized to the number of unpaired electrons. Dependence on ν_{xc}.

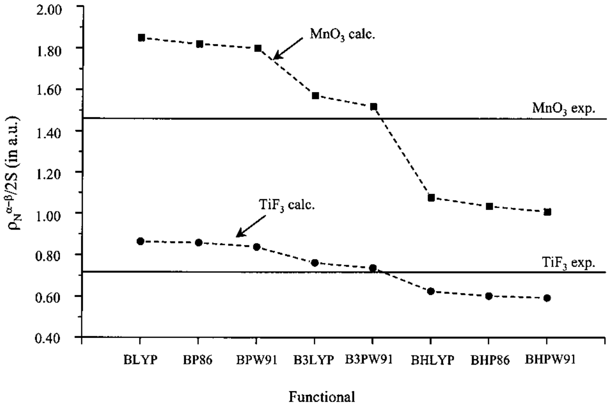

Figure 4. Spin density $\rho_N^{\alpha-\beta}$ at the metal nuclei in ^7MnF, ^7MnH, and $^6MnF_2$, normalized to the number of unpaired electrons. Dependence on ν_{xc}.

percent of the value of the HFCC (e.g., for ScO, TiN, TiO, or VO; note that previous studies have concentrated on such species), whereas for others this range may be on the order of the HFCC itself. This relative variation depends of course on the absolute value of the HFCC but also on other features we will discuss in more detail below. In comparison with experiment (Table 8), or with the coupled-cluster results (Table 3), unfortunately we cannot single out any functional which would be superior to the others. The performance of a given functional is very different for different classes of complexes. Thus, while the B3LYP functional has been particularly popular for HFCCs

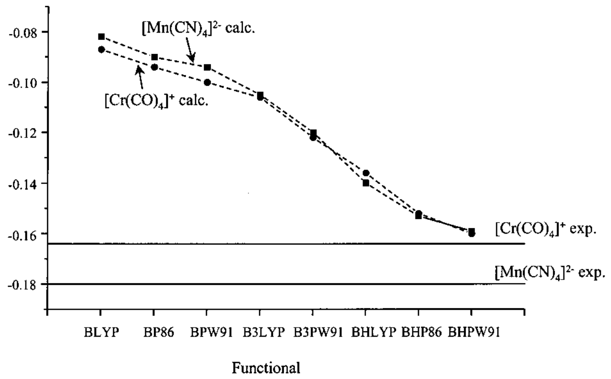

Figure 5. Spin density $\rho_N^{\alpha-\beta}$ at the metal nuclei in $^6[Mn(CN)_4]^{2-}$ and $^6[Cr(CO)_4]^+$, normalized to the number of unpaired electrons. Dependence on ν_{xc}.

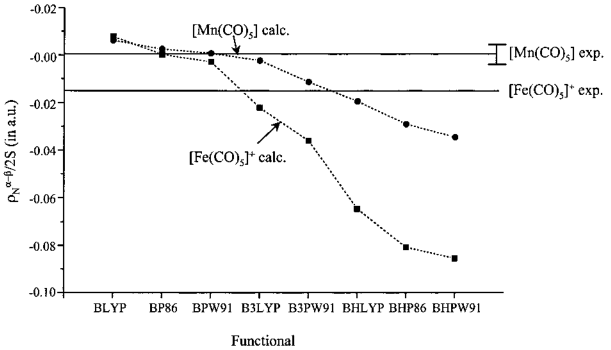

Figure 6. Spin density $\rho_N^{\alpha-\beta}$ at the metal nuclei in $^2[Mn(CO)_5]$ and $^2[Fe(CO)_5]^+$, normalized to the number of unpaired electrons. Dependence on ν_{xc}.

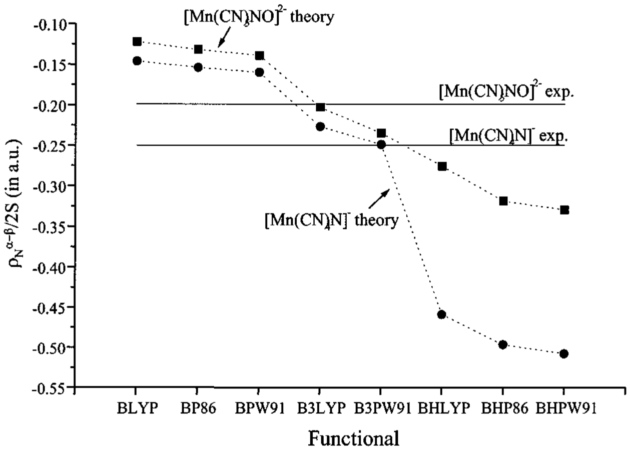

Figure 7. Spin density $\rho_N^{\alpha-\beta}$ at the metal nuclei in $^2[Mn(CN)_5NO]^{2-}$ and $^2[Mn(CN)_4N]^-$, normalized to the number of unpaired electrons. Dependence on ν_{xc}.

of organic molecules,[85] no “universal functional” appears to be available yet for the present transition metal systems.[86] The variations in the electronic structure appear to be too large. For the ”easier” systems mentioned (ScO, TiN, TiO, and VO), any of the GGA or hybrid functionals gives results within ca. 5−10% of the experimental values. In some cases (e.g., VN, MnO_3, $[Mn(CN)_4N]^-$, $[Ni(CO)_3H]$, $[Co(CO)_4]$), the spin contamination (cf. $<S^2>$ in Table 9) for the BH-type hybrid functionals is unacceptably large and leads to a deterioration of the results. In other cases (e.g., $[Mn(CN)_5NO]^{2-}$), spin contamination is even significant with pure GGA functionals. However, interestingly there is also a significant group of complexes (e.g., MnH, MnF_2, $[Mn(CN)_4]^{2-}$, $[Cr(CO)_4]^+$), where the half-and-half hybrids perform particularly well, without any apparent problems of spin contamination. Let us therefore discuss the results in more detail, and relate them to the electronic structure of the molecules in question.

ScO, TiN, TiO, VN, and VO. This first group of systems exhibits large positive spin density at the metal nucleus, resulting from the dominant participation of the metal 4s orbital in the SOMO, or in one of the SOMOs. ^{2}ScO and ^{2}TiN are the simplest representatives. Here the σ-type SOMO has predominantly metal 4s character,[9,12,29] with some $3d_{z^2}$ and 4p admixture (it is polarized away from the ligand). ^{3}TiO and ^{3}VN have in addition one $3d_\delta$-type SOMO, ^{4}VO two $3d_\delta$-type SOMOs. The dominance of the direct SOMO contribution to the HFCCs explains the relatively low dependence on ν_x (Figures 1, 2, Table 8). The treatment of dynamical correlation via ν_c appears to influence the HFCCs mainly via the shape of the SOMO. We find the SOMO to become more diffuse along the series LYP < P86 < PW91 (valence-shell spin polarization is also affected somewhat by ν_c). Addition of exact exchange also renders the SOMO somewhat more diffuse and reduces the HFCC slightly (the spin-polarization contributions are also affected but are not very pronounced).

VN is exceptional within this group, due to the significant onset of spin contamination upon inclusion of exact exchange (in contrast to the isoelectronic TiO!). This leads to a much larger dependence of the HFCC on the exchange functional, and finally to a significant deterioration of the results with BH-type hybrid functionals. This is confirmed by the results for A_{dip}(M) (Table 9). The relatively low coupling anisotropy is mainly due to the $3d_{z^2}$-type SOMO and depends relatively little on ν_{xc} for ScO, TiN, TiO, and VO. In contrast, for VN the admixture of exact exchange reduces the absolute value of A_{dip}(M) significantly, in parallel with the drastic increase in $<S^2>$ (Table 9). Unfortunately, no experimental A_{dip}(M) is available for this system.

^{3}TiO and ^{2}TiN have been studied recently by Engels et al.,[13] using the PWP86 functional and medium-sized basis sets. For TiN, their results differ only by ca. 1% from our BP86 value, despite their ca. 0.03 Å larger Ti−N distance. Our own test calculations for TiN at the structure used by Engels et al. indicate very small changes (<1 MHz), i.e., a small dependence of the isotropic metal HFCC on bond length. Recently, B3LYP calculations for ScO have been performed by Knight et al.[21] Their value given for A_{iso}(Sc) was 1877.5 MHz, ca. 8% lower than the value in Table 8, ca. 6% lower than our result with the larger 15s10p6d2f basis (cf. Table 6), but in excellent agreement with our B3PW91 results. Indeed, we have meanwhile been informed that Knight et al. erroneously reported their B3PW91 data as B3LYP results.[87]

Except for VN, the dipolar coupling constants (Table 9) are small and increase slightly in absolute value with increasing exact-exchange mixing in the functional. While this trend is partly related to an increasing participation of the metal $4p_z$ orbital in the SOMO, spin polarization should not be disregarded completely. Thus, e.g., a restricted B3PW91 calculation on ScO gives $A_{dip}(Sc) = +12.8$ MHz, quite different from the unrestricted result of +20.0 MHz. This should be compared to the RB3PW91 and UB3PW91 results for the isotropic HFCC of +1910.6 MHz and +1948.8 MHz, respectively. Thus, on a relative basis, spin polarization in ScO is more important for A_{dip}(Sc) than for A_{iso}(Sc)!

MnO, MnF$_2$, MnF, MnH. In going to higher spin multiplicities, we may compare ^{6}MnO to ^{4}VO. MnO has two additional SOMOs, antibonding orbitals with metal-$3d_\pi$ and $4p_\pi$, as well as ligand $2p_\pi$ character. Due to the large number of d-type

SOMOs, spin-polarization effects via the core shells are more pronounced. At first sight surprisingly, the BHLYP hybrid functional gives a somewhat larger spin density than B3LYP. This is most likely connected to the significant spin contamination upon exact-exchange mixing (cf. Table 9). The net dependence on ν_{xc} may still be considered moderate, with an overall range of less than 10% of the absolute HFCC. The somewhat larger dependence on ν_x and the spin contamination are also apparent from the somewhat larger variations in A_{dip}(M) compared to the above species (Table 9).

As related high-spin systems, but with lower net ρ_N, we may compare ^{7}MnF, ^{7}MnH, and ^{6}MnF$_2$ (cf. Figure 3, Table 8). ^{6}MnF$_2$ differs from the related ^{6}MnO by the symmetrical arrangement of two ligands in this linear two-coordinate complex. As a result, the single σ-type SOMO (which is accompanied by two 3d$_\delta$- and two 3d$_\pi$-type SOMOs) has larger 3d$_{z^2}$ and less 4s character than for MnO and is significantly Mn−F antibonding. The isotropic HFCC is therefore lower, and its significantly larger dependence on ν_x is mainly due to valence-shell spin polarization. The overall range of A_{iso}(M) values is thus larger than the relatively low HFCC itself. Comparison with experiment suggests the BH-type hybrid functionals to provide the best description (Table 8). Spin contamination is generally low. The absolute value of A_{dip}(M) is very small and thus difficult to describe accurately. Moreover, it changes significantly from Ne to Ar matrix (Table 9). Remember that this system was also one of the more difficult examples in the coupled cluster calculations (section 5, Table 3).

^{7}MnF and ^{7}MnH differ from ^{6}MnO and ^{6}MnF$_2$ mainly by having two rather than one singly occupied σ-type orbitals. The metal 4s orbital contributes in an Mn-X bonding way to one of these SOMOs, in an antibonding fashion to the other one (both orbitals are again dominated by the 3d$_{z^2}$ orbital). As for MnF$_2$, inclusion of exact exchange influences mainly the SOMO and valence-shell spin-polarization contributions in both systems, while the total core polarizations are almost unaffected. The overall dependence on ν_x is quite large for MnH (but not as large as for MnF$_2$), somewhat lower for MnF (cf. Figure 3). The choice of ν_c influences both core and valence shell contributions. For MnH these changes cancel each other so that the overall dependence on ν_c is low, similar to MnF$_2$ but in contrast to MnF. The comparison with experiment would suggest BH-type functionals to perform best for MnH. On the other hand, all functionals give results within ca. 13% from experiment for MnF. Spin contamination does not seem to be a problem for MnF$_2$, MnF, or MnH, in contrast to the BH-type results for MnO (Table 9).

For these four manganese systems, A_{dip}(M) is very small and caused mainly by the 3d$_{xz}$, 3d$_{yz}$, 3d$_{xy}$, and 3d$_{x^2-y^2}$ character of the π- and δ-type SOMOs. It is notable that the effect of spin polarization is again not negligible (cf. above). For example, the dipolar coupling of −15.7 MHz for MnO at the unrestricted BHPW91 level is changed to −20.2 MHz at the restricted level. Similarly, we obtain +2.4 MHz for A_{dip}(Mn) in MnF$_2$ at the unrestricted, −5.9 MHz at the restricted BHPW91 level.

TiF$_3$ and MnO$_3$. Two related molecules with relatively large positive spin densities at the nuclei, but with a significant dependence on ν_{xc} are TiF$_3$ and MnO$_3$ (cf. Figure 4, Table 8). For both systems, the SOMO is dominated by the metal 3d$_{z^2}$ orbital, interacting with the ligand hybrid orbitals in an antibonding way. Some 4s character is mixed in. The composition of the SOMO is similar for both complexes (Mulliken population analyses, using the BLYP functional, give a 4s/3d$_{z^2}$ population ratio of 0.18/0.76 for TiF$_3$ and of 0.13/0.67 for MnO$_3$). The larger ρ_N of MnO$_3$ is thus due to the much larger effective charge on the metal. The sensitivity to ν_x is already significant for TiF$_3$, but all functionals do still give results within ca. 15% of the experimental value. DFT calculations of Belanzoni et al.[17] (with the BP86 functional and STO basis sets) gave −233.9 MHz for A_{iso}(Ti), somewhat larger than our −216.6 MHz with the same functional. This difference arises mainly from their shorter LSDA Ti−F bond length (1.756 Å vs our 1.780 Å). Using their shorter distance, we obtain −231.0 MHz, i.e., closer agreement with their value (note the negative g_N(Ti), Table 7). This indicates a much larger structural dependence of A_{iso}(Ti) compared to our above discussion for TiN, probably due to presence of core−shell spin-polarization contributions.

In view of the significant deviations of the g-tensor from the free-electron value (Table 2), TiF$_3$ is one of the cases where spin−orbit effects have to be considered. Indeed, here we are in the fortunate situation that explicit DFT calculations of these spin−orbit contributions are available, both within a perturbation−theoretical approach,[17] and using the explicitly relativistic two-component zero-order-regular-approximation (ZORA) scheme.[19] Using the BP86 functional, both approaches gave very small positive spin−orbit (pseudocontact) contributions to A_{iso}(Ti) (ca. 3−6 MHz), whereas the spin−orbit contributions to A_{dip}(Ti) are negative (between −2.3 MHz and −2.8 MHz) and significant relative to the small dipolar coupling. Our own simple semiempirical estimate of the spin−orbit corrections (section 4, eq 6) gives +3.4 MHz for the pseudocontact term and −2.1 MHz for A_{dip}, in good agreement with the explicit calculations. The addition of the latter value to the computed A_{dip} does not improve the agreement with experiment, but it has to be noted that the matrix does affect the results nonnegligibly (cf. Table 9).

For MnO$_3$, the ν_x dependence of A_{iso} is particularly pronounced (Table 8 and Figure 4), and is complicated by significant spin contamination (cf. $\langle S^2 \rangle$ and the large dependence of A_{dip}(Mn) on ν_x, Table 9). The results for MnO$_3$ exemplify a dilemma that arises also in other cases (see below): While some admixture of exact exchange increases spin polarization and thus may improve the agreement with experiment relative to the ”pure” GGA results, it may lead at the same time to considerable spin contamination (we note that the spin contamination is connected to valence-shell spin polarization.). Thus, despite the superficial similarity with the isoelectronic TiF$_3$, the demands on the functional are much higher for the more covalent, highly oxidized MnO$_3$ (cf. also the VN vs TiO comparison above). One could argue that the B3-type functionals do still provide a reasonable description of the wave function for MnO$_3$ (with moderate but nonnegligible spin contamination). However, the unusually large variations in A_{dip}(M) (Table 9) speak against this. Note that the coupled cluster results for A_{iso}(M) (Table 3) agree well with experiment (they are slightly too negative).

[Mn(CN)$_4$]$^{2-}$ and [Cr(CO)$_4$]$^+$. As two further high-spin systems, we may examine the two isoelectronic, tetrahedral ions ^{6}[Mn(CN)$_4$]$^{2-}$ and ^{6}[Cr(CO)$_4$]$^+$. The five SOMOs correspond to all five metal d orbitals, corresponding to the t_2 and e irreducible representations in T_d symmetry. Due to the absence of any direct s-type SOMO contribution, ρ_N is entirely caused by spin polarization and is negative for both systems (see Figure 5; the positive A_{iso}(Cr) is due to the negative g_N(Cr), cf. Table 7). Spin polarization of the core shells by the d-type SOMOs dominates (and provides negative ρ_N) and is partly compensated by valence-shell spin polarization. Therefore, the dependence on ν_{xc} is particularly large, and it is rather similar for these isoelectronic systems (Figure 5). Even with BH-type hybrid functionals, which provide the best agreement with experiment, the spin polarization apparently is still underestimated slightly. The coupling anisotropy is zero, due to symmetry, and spin contamination is relatively small for all functionals (Table 9).

[Mn(CO)$_5$] and [Fe(CO)$_5$]$^+$. Let us now turn to low-spin complexes. For the isoelectronic low-spin d^7 complexes ^{2}[Mn(CO)$_5$] and ^{2}[Fe(CO)$_5$]$^+$, the SOMO exhibits metal 3d$_{z^2}$ and 4p$_z$ character and is σ-antibonding with respect to the axial M-CO bond in these square pyramidal (C_{4v}) complexes. The metal 4s contribution to the SOMO is small. As the small positive direct SOMO contribution to A_{iso}(M) (ca. +60 MHz and ca. +14 MHz for M = Mn, Fe, respectively) is furthermore canceled partly by negative core−shell spin-polarization contributions, very small isotropic HFCCs result for these low-spin systems. As a consequence, the description is difficult and the dependence on ν_{xc} (particularly on ν_x) is large on a relative scale (Figure 6). This holds in particular for the iron complex. In other words, a larger effective charge at the metal appears to increase the sensitivity to the functional (as found above for other isoelectronic pairs, e.g., VN vs TiO or MnO$_3$ vs TiF$_3$). Based on the comparison to experiment, it is difficult to select any particular functional that would be preferable over the others (the BH-type hybrids might seem to be less preferable, although spin contamination is not very pronounced). We estimate spin−orbit corrections (cf. section 4) of ca. +21.2 MHz for A_{iso}(Mn) and of ca. −12.8 MHz for A_{dip}(Mn) in [Mn(CO)$_5$], as well as ca. +5.3 MHz for A_{iso}(Fe) and ca. −3.0 MHz for A_{dip}(Fe) in [Fe(CO)$_5$]$^+$. The correction for the manganese complex may be overestimated, as the coefficient of the 3d$_{z^2}$ orbital in the SOMO is small (δ^2 = 0.43, cf. eq 6) and the neglected contribution from the 4p$_z$ orbital may be large.

[Mn(CN)$_5$NO]$^{2-}$ and [Mn(CN)$_4$N]$^-$. The two C_{4v} symmetrical systems ^{2}[Mn(CN)$_5$NO]$^{2-}$ and ^{2}[Mn(CN)$_4$N]$^-$ (a low-spin d^5 and a d^1 complex, respectively) both have a single metal 3d$_{xy}$-type SOMO. They also share the unfortunate problem of significant spin contamination, in particular with hybrid functionals (Table 9). Significant core−shell spin polarization dominates the observed negative isotropic HFCCs. This is augmented by valence-shell spin polarization, mainly involving metal d$_{xz}$ and d$_{yz}$ orbitals. These d-orbitals contribute to the π-components of the Mn−N triple bond in the d^1 system, and to both Mn−N π-bonding and π-antibonding MOs in the d^5 complex. Low-lying excited states involving these π- and π*-type orbitals are mainly responsible for the spin contamination (i.e., the spin contamination is connected to significant valence-shell spin polarization, as found above for MnO$_3$).

Spin contamination is already nonnegligible for the GGA functionals, increases for the B3-type hybrids, and becomes dramatic for the BH-type hybrids. As a consequence, the computed A_{dip} values appear to be still reasonable for the GGAs but deteriorate significantly for the hybrid functionals (with the exception of the B3-type hybrid results for [Mn(CN)$_4$N]$^-$). The isotropic HFCCs are not sufficiently negative with the GGAs, are in closer agreement with experiment for the B3-type hybrids, but become much too negative with the BH-type hybrids (Figure 7). We have to conclude that the reasonable A_{iso} results with the B3-type hybrids are at least in part fortuitous, due to spin contamination. None of the functionals investigated here is thus really adequate to describe all features of the hyperfine coupling in these two complexes. We also note that SCF convergence to a global minimum in parameter space (i.e., in the MO coefficients) was difficult with several of the functionals, in particular for [Mn(CN)$_4$N]$^-$. It appears that low-lying local minima exist. We have therefore used tighter convergence criteria on the density matrix for these systems than the *Gaussian 94* default values (i.e., 10^{-8} au instead of 10^{-4} au root-mean-square deviation).

The pure GGA functionals give three positive occupied orbital energies for [Mn(CN)$_5$NO]$^{2-}$ (no positive eigenvalues are obtained with the BH-type hybrids), indicating that the isolated dianion might not be stable with respect to electron loss (this holds also for the [Mn(CN)$_4$]$^{2-}$ dianion discussed above). However, we believe that, in connection with the finite basis set, this affects the HFCC results negligibly compared to the more serious problem of spin contamination.

Due to the significant deviations of the g-tensor components from the free-electron value (Table 2) in [Mn(CN)$_5$NO]$^{2-}$, we have considered spin−orbit corrections. Our simple estimate gives a pseudocontact term of ca. +6.4 MHz and a spin−orbit contribution to A_{dip} of −2.8 MHz. Spin−orbit effects are estimated to be small for [Mn(CN)$_4$N]$^-$ (cf. g-tensor in Table 2).

[Ni(CO)$_3$H] and [Co(CO)$_4$]. The SOMO of these two trigonal pyramidal (C_{3v}) d^9 complexes[88] is of a_1 symmetry and composed of metal 3d$_{z^2}$ and 4p$_z$ contributions, with overall axial metal−ligand σ-antibonding character. In both cases, the SOMO has very little metal 4s character and thus gives only small direct contributions to ρ_N. These are furthermore compensated partially by the negative core−shell spin polarization. As a result, the isotropic HFCCs are low. Possibly due to the partial 4p$_z$ character of the SOMO, the dipolar couplings are relatively large (in analogy to the low-spin d^7 complexes [Mn(CO)$_5$] and [Fe(CO)$_5$]$^+$ discussed above).

At first sight, A_{dip}(M) in [Co(CO)$_4$] would seem significantly too large with GGA (and B3-type) functionals (Table 9), despite the relatively small spin contamination. However, in view of the very large g-shifts (Table 2), spin−orbit corrections are expected to be particularly significant for this complex. Indeed, our simple estimate (eq 6, section 4) provides a large correction of −42.2 MHz to A_{dip}(Co). This would bring both the GGA results and the B3-type hybrid results into good agreement with experiment, whereas the BH-type hybrid results would then be too low. The reduction of the dipolar couplings by inclusion of exact exchange is again accompanied by signifcant spin contamination, and we do not expect these BH-type functionals to provide a reliable description for this system. In view of its smallness, the isotropic HFCC (Table 8) is difficult to describe. Considering also the estimated spin−orbit correction to A_{iso}(Co) of +69.5 MHz may suggest that even the B3-type hybrid results are still insufficiently negative. On the other hand, the BH-type hybrid results clearly overshoot the negative spin-polarization contributions dramatically.

Both spin contamination and the dependence of A_{dip}(M) on ν_{xc} are less pronounced for [Ni(CO)$_3$H]. The GGA results would seem to agree best with experiment for A_{dip}(Ni), whereas the BH-type hybrid results are clearly too negative (and are accompanied by spin-contamination, Table 9). Our estimated spin−orbit correction of +16.4 MHz to A_{dip}(Ni) would change this picture but may be too large, as the metal 4p$_z$ orbital contributes significantly to the SOMO (the 3d$_{z^2}$ contribution to the SOMO is particularly low for this complex, with δ^2 = 0.28, cf. eq 6). The estimated spin−orbit correction to A_{iso}(Ni) (pseudocontact term) of −26.8 MHz may thus also be too large. In view of these uncertainties about the magnitude of the spin−orbit corrections, either GGA or B3-type hybrid functionals might be closest to the experimental isotropic HFCC (Table 8), whereas the BH-type hybrids give in any case too large values.

CuO. The d^9 complex ^{2}CuO differs from the previous cases by exhibiting a hole in a degenerate (π-type) MO. In other words, the one-particle description of the $X^2\Pi$ ground state of CuO assigns three electrons to the 4π MO (the two components are built from the O $2p_x$, Cu $3d_{xz}$, Cu $4p_x$, and from the O $2p_y$, Cu $3d_{yz}$, and Cu $4p_y$ orbitals, respectively).[89] It is thus clear that a cylindrically symmetrical wave function in a single-determinant framework may be obtained only by using fractional occupations (i.e., 0.5 electrons in each of the two MOs). The integer occupation of one of the two degenerate 4π MOs would, e.g., not provide an axially symmetrical hyperfine tensor. On the other hand, one may average calculations with different integer occupations (similar considerations pertain to Kohn−Sham calculations on certain degenerate states of open-shell atoms[90a]). The results for A_{dip}(Cu) obtained by this averaging procedure are given in Table 9 (the coupled cluster results in Table 3 were obtained in the same manner). As we were not able to enforce appropriate fractional occupations within the *Gaussian 94* program, we resorted to calculations using the BP86 functional and the deMon code[31,90] to compare integer and fractional occupations (using the same basis set but in addition auxiliary basis sets to fit charge density and exchange−correlation potential[31,90]). Indeed, the dipolar couplings obtained with fractional occupations differed by less than 6 MHz from averaged results with integer occupations (the isotropic couplings also changed by less than 5 MHz). This seems to justify the averaging procedure.

Due to the absence of metal 4s orbital contributions to the SOMO, the isotropic metal HFCC arises exclusively from spin polarization. Interestingly, the ν_x dependence for a given ν_c is $\rho_N(B) > \rho_N(BH) > \rho_N(B3)$. On the other hand, we find a significant decrease of A_{dip}(Cu) from B to B3 to BH functionals. The latter trend is due to the shift of single-electron density from Cu to O with admixture of exact exchange. For the isotropic HFCCs, stronger core−shell spin polarization accounts for the more negative value with B3-type relative to B-type functionals. Further dramatic decrease of the spin density on Cu reverses the trend and gives a less negative A_{iso}(Cu) with BH-type functionals.

The A_{iso}(Cu) results are too negative for all functionals, whereas the variation between the functionals is smaller than the discrepancy with respect to experiment. Note that even the coupled cluster calculations give too negative A_{iso}(Cu) when considering the trend upon enlarging the basis set (Table 3). Moreover, spin contamination seems to be small. The difference with respect to experiment is thus probably not mainly a problem of describing the spin polarization well. There are three other possible reasons which might account for the too negative isotropic HFCCs, of which we suspect the latter to be decisive: multireference character of the wave function, errors in the bond length, relativistic effects.

Multireference Character of the Wave Function. Our coupled cluster wave functions give no large coefficients for configurations other than the given reference configuration. We note also that the single-reference coupled-pair-functional (CPF) calculations by Langhoff and Bauschlicher appear to describe the ground state of CuO adequately (whereas CISD calculations without corrections for higher order excitations perform poorly).[91] Thus, CuO is probably not a priori a multireference case. Moreover, spin contamination is small. This speaks against significant problems of describing the wave function with the current approaches.

Bond Length Errors. The isotropic HFCC is extremely dependent on the Cu−O bond length. Shortening the bond by only 0.005 Å (from 1.729 to 1.724 Å) changes A_{iso}(Cu) from −776 MHz to −747 MHz, i.e., by ca. 4% (B3PW91 result). Together with the above results for TiN and TiF_3, this suggests that the dependence of the isotropic HFCCs on bond length increases with an increasing importance of spin polarization (a more systematic study of the interdependence between structural changes and HFCCs in transition metal complexes is beyond the scope of the present study but should be pursued in the future). On the other hand, the experimental bond distance of 1.729 Å appears to be reliable and has been confirmed experimentally[92] and theoretically.[93]

Relativistic Effects. Scalar relativistic effects should lead to a larger (negative) spin density at the nucleus and would thus be expected to lead to *more* negative values for A_{iso}(Cu). Spin−orbit effects are difficult to judge, as unfortunately no experimental g-tensor information is available. Our preliminary perturbation−theoretical calculations of the g-tensor indicate a large positive $\Delta g_{\perp}$. Thus, we may expect significant spin−orbit contributions to the HFCCs, and we believe that this is the most likely reason for the discrepancies between calculation and experiment.

[Cu(CO)$_3$]. Finally, we look at a very different bonding situation. The wave function in [Cu(CO)$_3$] is derived from the $3d^{10}4p^1$ configuration of Cu^0, and the SOMO is composed of the Cu $4p_z$ orbital and π-type ligand orbitals. The isotropic metal HFCC is thus exclusively due to spin polarization. Interestingly, ρ_N(Cu) is positive, whereas we have seen above that core−shell spin polarization due to 3d-type SOMOs always contributes negatively to ρ_N(M). Thus, the situation resembles more that known for main-group π-type radicals, with the (slight) difference that we have a very polarizable M-shell below the $4p_z$-type SOMO. The description for [Cu(CO)$_3$] is thus considerably more difficult than for Cu(C_2H_2) or Cu(CO) studied previously with DFT methods by Barone et al.,[14,15] where large positive direct contributions from a metal 4s-type SOMO dominate.

Spin contamination is minor, and the dipolar couplings depend relatively little on the functional (however, the BH-type hybrids give ca. 6−7 MHz lower values, cf. Table 9). The experimental A_{dip}(Cu) is underestimated. It is possible that this is due to an overestimate of the Cu−C bond length even by the MP2 optimizations used (cf. Table 1). This would be consistent with our finding that test calculations at the larger DFT optimized bond length (also Table 1), give ca. 8 MHz lower dipolar couplings. In other words, structural errors are more likely for this weakly bound complex than for the other systems.

Looking at the isotropic metal HFCC (Table 8), we see that we obviously underestimate core−shell spin polarization with the pure GGA functionals. Even the sign of the HFCC is wrong. The agreement with experiment is improved somewhat with B3-type hybrids, and even more significantly with the BH-type hybrids, without any apparent spin contamination problem. The situation may thus be comparable to that for π-type organic radicals.[15] We also see a surprisingly large difference between the BHLYP functional and the BHP86 and BHPW91 functionals (likely due to the description of the SOMO).

8. Ligand HFCCs

As this work concentrates on complexes with the SOMO mainly localized on the metal, the spin densities at the ligand nuclei are about 1−2 orders of magnitude smaller than those at the metal nuclei. This places of course considerable demand

TABLE 10: Isotropic Ligand HFCCs (in MHz)

	isotope	BLYP	BP86	BPW91	B3LYP	B3PW91	BHLYP	BHP86	BHPW91	exp[a]
^{2}ScO	^{17}O	−22.8	−21.3	−19.8	−19.9	−17.0	−16.5	−13.3	−11.6	−20.3(3) or −18.9(4)[b,c]
^{2}TiN	^{14}N	19.8	18.4	17.3	17.1	14.4	12.8	10.1	9.5	18.478(1)
^{3}TiO	^{17}O	−8.2	−8.2	−7.3	−4.9	−4.3	−0.2	0.6	1.6	
^{3}VN	^{14}N	6.0	6.2	5.8	3.2	3.2	−9.3	−6.0	−7.2	
^{4}VO	^{17}O	−2.7	−3.1	−2.4	1.1	1.5	6.7	7.3	8.0	0(4)[d]
^{6}MnO	^{17}O	−6.6	−5.4	−5.3	−8.0	−7.3	−9.0	−9.1	−8.8	
^{6}MnF$_2$	^{19}F	20.4	16.1	15.4	22.6	18.5	27.9	20.4	20.8	
^{7}MnF	^{19}F	78.5	69.4	67.2	79.2	72.9	82.9	79.5	77.9	68(6) or 75(6)[b]
^{7}MnH	^{1}H	35.6	25.8	22.1	28.0	19.0	23.0	14.0	10.1	20.7(39)
^{2}TiF$_3$	^{19}F	8.7	5.0	1.7	−5.6	−12.9	−14.8	−23.5	−24.3	8.3(4) or 8.0(4)[b,e]
^{2}MnO$_3$	^{17}O	−5.1	−4.1	−3.5	2.6	2.6	26.2	19.1	19.0	
^{6}[Mn(CN)$_4$]$^{2-}$	^{13}C	3.5	−0.1	−0.8	0.5	−3.0	−1.2	−4.7	−5.1	
	^{14}N	1.1	0.8	0.7	1.0	0.8	1.1	0.8	0.8	
^{6}[Cr(CO)$_4$]$^{+}$	^{13}C	−5.0	−9.2	−11.5	−8.4	−13.4	−10.4	−14.6	−15.4	−13.5
	^{17}O	−1.6	−1.2	−1.1	−1.8	−1.4	−2.1	−1.7	−1.6	
^{2}[Mn(CO)$_5$]	^{13}C$_{ax}$	0.7	−1.9	−3.4	−34.4	−37.0	−72.7	−72.9	−73.0	
	^{13}C$_{eq}$	−15.1	−18.3	−19.7	−21.7	−26.0	−27.9	−31.2	−32.2	
	^{17}O$_{ax}$	−8.8	−8.2	−8.0	−8.2	−7.6	−6.4	−6.1	−5.8	
	^{17}O$_{eq}$	−2.9	−2.0	−2.0	−3.6	−2.7	−4.3	−3.6	−3.2	
^{2}[Fe(CO)$_5$]$^{+}$	^{13}C$_{ax}$	69.7	65.6	65.0	39.0	37.0	20.5	18.8	20.2	53.5
	^{13}C$_{eq}$	−18.5	−20.3	−21.3	−25.1	−26.9	−25.2	−27.0	−26.9	−23.0
	^{17}O$_{ax}$	−9.6	−9.2	−9.1	−9.9	−9.6	−9.3	−9.2	−9.0	
	^{17}O$_{eq}$	−1.9	−1.4	−1.4	−1.7	−1.3	−1.2	−1.0	−0.8	
^{2}[Mn(CN)$_5$NO]$^{2-}$	^{13}C$_{ax}$	−44.4	−41.3	−43.9	−83.3	−88.0	−136.6	−133.2	−130.7	
	^{13}C$_{eq}$	−41.6	−40.1	−42.9	−80.4	−85.4	−133.2	−132.1	−128.2	
	^{14}N(NO)	−12.3	−9.7	−10.6	−29.6	−27.5	−55.7	−50.0	−49.9	−10.64
	^{14}N(CN$_{ax}$)	0.5	0.4	0.4	0.7	0.6	0.9	0.4	0.6	
	^{14}N(CN$_{eq}$)	1.0	0.5	0.5	1.0	0.7	1.2	0.7	0.6	
	^{17}O	7.8	4.0	4.3	33.2	27.6	82.0	70.5	69.7	
^{2}[Mn(CN)$_4$N]$^{-}$	^{13}C	−28.9	−28.7	−30.1	−53.0	−55.4	−135.1	−134.1	−136.2	
	^{14}N$_{ax}$	−3.1	−1.5	−1.4	−8.2	−5.0	−31.3	−21.3	−19.4	
	^{14}N$_{eq}$	1.4	0.7	0.7	1.8	1.3	3.6	2.7	2.8	
^{2}[Ni(CO)$_3$H]	^{1}H	348.2	308.7	311.8	208.0	189.3	−116.2	−105.5	−110.0	293
	^{13}C	17.3	12.4	11.9	5.1	4.8	−8.3	−10.7	−10.2	
	^{17}O	−3.0	−2.2	−2.2	−3.7	−3.1	−4.1	−3.6	−3.5	
^{2}[Co(CO)$_4$]	^{13}C$_{ax}$	105.8	101.0	100.4	57.3	55.6	29.7	32.8	37.7	67.2
	^{13}C$_{eq}$	6.2	3.2	3.1	3.0	1.5	15.6	18.8	24.7	
	^{17}O$_{ax}$	−13.7	−13.1	−12.9	−12.7	−12.1	−9.0	−8.8	−8.3	
	^{17}O$_{eq}$	−2.9	−2.4	−2.4	−2.9	−2.7	−1.2	−1.3	−0.7	
^{2}CuO	^{17}O	−20.4	−6.7	−5.2	−32.0	−18.7	−55.7	−39.2	−37.9	
^{2}[Cu(CO)$_3$]	^{13}C	−6.3	−14.6	−17.5	−12.3	−20.5	−19.1	−30.4	−32.3	−18.7
	^{17}O	−4.4	−2.7	−2.7	−6.9	−5.3	−10.7	−11.3	−9.0	11.2

[a] Unless stated otherwise, the experimental values are from the sources cited in the corresponding footnotes to Table 8. [b] In Ne or Ar matrix, respectively. [c] Cf. ref 10. [d] In Ne matrix, ref 12. [e] Reference 44, cf. ref 18 for a revision.

on the computational approach to describe the subtle delocalization of spin density to the ligands, as well as spin-polarization effects. We should also mention again that relativistic effects, which are not considered here, may have a nonnegligible influence on the small ligand HFCCs (cf. section 4). The metal HFCCs are our main interest in this work, but we may nevertheless note some trends in the computed ligand HFCCs.

Table 10 summarizes the isotropic ligand HFCCs, Table 11 the dipolar couplings. Concerning the dependence of the isotropic HFCCs on ν_{xc}, we note trends very similar to above for the metal HFCCs. Thus, the spin densities ρ_N at the ligand nuclei (when including their signs) exhibit often the ν_c dependence $\rho_N(\mathrm{LYP}) \geq \rho_N(\mathrm{P86}) \geq \rho_N(\mathrm{PW91})$ for a given ν_x, and typically the ν_x dependence $\rho_N(\mathrm{B}) \geq \rho_N(\mathrm{B3}) \geq \rho_N(\mathrm{BH})$ for a given ν_c (the negative $g_N(\mathrm{O})$ needs to be kept in mind, cf. Table 7). A notable exception to this trend is provided by the inverse dependence on ν_x, i.e., $\rho_N(\mathrm{BH}) \geq \rho_N(\mathrm{B3}) \geq \rho_N(\mathrm{B})$ in the high-spin complexes MnO, MnF$_2$, and MnF or in the case of ^{17}O splitting in CuO and Cu(CO)$_3$. Exceptions to the abovementioned trends are also notable when significant spin contamination is connected to orbitals with large contributions on the given ligand (see, e.g., results for VN, MnO$_3$, [Co(CO)$_4$]), and for the axial nitrogen in [Mn(CN)$_4$N]$^-$ (cf. Table 10). The relative sensitivity of the results to ν_x vs ν_c is of course different than it was for the metal HFCCs, as the relevant spin-polarization effects are now those around the ligand nuclei.

As for the isotropic metal HFCCs, the isotropic ligand HFCCs are made up of direct SOMO and indirect spin-polarization contributions. The latter are missing for MnH, where the single hydrogen 1s-AO is directly involved in two of the SOMOs (cf. section 7). The A_{iso}(H) in MnH is thus a relatively simple measure of the localization of the two σ-type SOMOs at the H nucleus. Interestingly, the dependence of this A_{iso}(H) on ν_{xc} in MnH is similar to that of the metal HFCCs in ScO and TiN, which are also dominated by direct SOMO contributions (but with much larger overall ρ_N; cf. section 7). The significant difference between LYP and the two other correlation functionals is particularly notable for A_{iso}(H) in MnH. This may suggest that the description of dynamical correlation is critical for the charge distribution within the two σ-type SOMOs.

A similar dependence on ν_c is apparent for the ^{13}C HFCCs in [Mn(CN)$_4$]$^{2-}$ and [Cr(CO)$_4$]$^+$, but for a different reason: The SOMO contributions are affected very little, and it is valence-shell spin polarization which changes with ν_c (core polarizations at carbon are negligible). Experimental data are available only for [Cr(CO)$_4$]$^+$. The hybrid functionals appear to give better

TABLE 11: Dipolar Ligand HFCCs (in MHz)[a]

	isotope	BLYP	BP86	BPW91	B3LYP	B3PW91	BHLYP	BHP86	BHPW91	exp[b]
^{2}ScO	^{17}O	0.2	−0.2	−0.2	0.6	0.2	1.4	0.7	0.7	0.4(2), 0.7(3)[c]
^{2}TiN	^{14}N	0.6	0.5	0.4	0.4	0.3	0.0	−0.1	−0.3	0.055(2)
^{3}TiO	^{17}O	−1.1	−1.5	−1.6	−0.6	−1.0	0.7	0.4	0.3	
^{3}VN	^{14}N	1.7	1.7	1.7	2.1	2.2	3.6	3.9	3.9	
^{4}VO	^{17}O	−2.2	−2.8	−3.1	−1.7	−2.5	0.0	−0.3	−1.1	0(3)
^{2}TiF$_3$	^{19}F[d]	20.9, −0.2, −20.7	26.9, 5.0, −31.9	29.7, 6.4, −35.8	19.4, −0.4, −19.0	25.2, 4.8, −30.0	15.7, 2.2, −13.4	19.6, 2.0, −21.6	21.6, 2.8, −24.4	*e*
^{2}MnO$_3$	^{17}O[d]	−23.9, 3.0, 20.9	−24.2, 2.0, 22.2	−24.7, 1.5, 23.2	−34.7, −14.9, 49.6	−55.3, 18.1, 37.2	−61.7, −57.2, 118.9	−61.5, −57.8, 119.3	−62.1, −57.9, 120.0	
^{6}[Mn(CN)$_4$]$^{2-}$	^{13}C	2.1	2.0	2.0	2.0	2.0	2.1	2.0	2.0	
	^{14}N	−0.1	−0.1	−0.1	−0.1	−0.1	−0.1	−0.1	−0.1	
^{6}[Cr(CO)$_4$]$^{+}$	^{13}C	1.1	1.1	0.8	1.4	1.1	1.4	1.4	1.4	1.0
	^{17}O	1.0	0.8	1.0	0.9	0.9	0.8	0.8	0.8	
^{6}MnO	^{17}O	8.3	8.1	8.3	9.9	10.1	15.4	15.5	15.7	
^{6}MnF$_2$	^{19}F	−19.3	−18.9	−18.3	−15.7	−15.3	−11.8	−11.7	−11.6	
^{7}MnF	^{19}F	12.9	13.4	13.7	13.4	13.4	12.9	12.6	12.6	8(6), 10(6)[c]
^{7}MnH	^{1}H	10.9	10.9	10.9	11.2	11.2	11.8	11.8	11.8	8.4(33)
^{2}[Mn(CO)$_5$]	^{13}C$_{ax}$	1.6	1.2	1.6	1.1	1.1	0.7	0.7	0.8	
	^{13}C$_{eq}$[f]	−0.8, −5.8, 6.7	−0.8, −5.6, 6.5	−0.8, −5.7, 6.6	−0.5, −5.6, 6.1	−0.2, −5.6, 5.8	−0.3, −5.4, 5.6	−0.3, −5.4, 5.6	−0.3, −5.5, 5.7	
	^{17}O$_{ax}$	−2.0	−2.0	−2.1	−1.7	−1.8	−1.7	−1.7	−1.9	
	^{17}O$_{eq}$[f]	7.0, 8.6, −15.6	6.9, 8.3, −15.2	6.8, 8.3, −15.1	6.7, 8.9, −15.6	6.3, 8.8, −15.1	5.5, 10.6, −16.1	5.4, 10.2, −15.6	5.1, 10.3, −15.4	
^{2}[Fe(CO)$_5$]$^{+}$	^{13}C$_{ax}$	2.8	2.8	2.8	2.0	2.0	1.4	1.4	1.4	2.8
	13C$_{eq}$[f]	5.0, −3.6, −1.4	4.9, −3.5, −1.3	5.0, −3.6, −1.4	5.4, −3.1, −2.2	5.3, −3.1, −2.2	5.8, −3.1, −2.7	5.7, −3.1, −2.7	5.8, −3.0, −2.8	4.4, −2.2, −2.2
	^{17}O$_{ax}$	−3.0	−3.0	−3.0	−2.6	−2.7	−2.7	−5.0	−2.8	
	^{17}O$_{eq}$[f]	3.2, 5.1, −8.3	3.2, 5.0, −8.2	3.2, 4.9, −8.1	2.2, 4.8, −7.0	2.1, 4.7, −6.9	0.9, 4.9, −5.8	1.0, 4.8, −5.8	0.9, 4.8, −5.6	
^{2}[Mn(CN)$_5$NO]$^{2-}$	^{13}C$_{ax}$	1.1	1.1	1.1	2.2	2.2	3.0	2.9	3.0	
	^{13}C$_{eq}$[f]	5.1, −3.1, −2.0	5.0, −3.1, −1.9	5.1, −3.2, −1.9	6.3, −4.2, −2.1	6.3, −4.2, −2.1	6.7, −5.0, −1.7	6.6, −5.0, −1.7	6.7, −5.0, −1.7	
	^{14}N(NO)	7.9	7.1	7.7	17.7	17.7	23.9	23.1	23.5	2.7
	^{14}N$_{ax}$(CN)	−0.6	−0.6	−0.6	−1.2	−1.3	−1.8	−1.8	−1.7	
	^{14}N$_{eq}$(CN)[f]	−2.9, 4.6, −1.7	−2.9, 4.7, −1.8	−3.0, 4.7, −1.7	−3.2, 4.1, −0.9	−3.4, 4.2, −0.8	−3.9, 4.4, −0.5	−3.9, 4.4, −0.5	−3.9, 4.4, −0.5	
	^{17}O	−15.0	−13.6	−14.6	−38.2	−38.3	−55.0	−54.3	−54.2	
^{2}[Mn(CN)$_4$N]$^{-}$	^{13}C[f]	5.0, −2.7, −2.3	5.0, −2.7, −2.3,	5.1, −2.8, −2.3	6.4, −4.4, −2.0	6.5, −4.5, −2.0	8.7, −3.7, −3.1	8.6, −5.0, −3.6	8.9, −5.2, −3.7	
	^{14}N$_{ax}$	2.4	2.4	2.5	6.6	6.9	16.9	16.9	16.6	
	^{14}N(CN)[f]	−3.5, 5.8, −2.3	−3.5, 5.8, −2.2	−3.6, 5.8, −2.2	−3.8, 4.8, −1.0	−3.9, 4.8, −0.9	−4.4, 5.9, −1.5	−4.4, 6.0, −1.6	−6.2, 7.9, −1.7	
^{2}[Ni(CO)$_3$H]	^{1}H	2.9	2.7	2.7	6.3	6.2	17.1	16.9	17.1	5.5
	^{13}C[f]	−2.6, −5.7, 8.3	−2.7, −5.6, 8.3	−2.8, −5.7, 8.5	−3.2, −5.5, 8.7	−3.3, −5.5, 8.8	−3.3, −5.3, 8.5	−3.2, −5.2, 8.5	−3.3, −5.4, 8.7	
	^{17}O[f]	−6.2, −8.4, 14.6	−6.3, −8.2, 14.4	−6.2, −8.2, 14.4	−5.3, −8.7, 14.0	−5.3, −8.6, 13.9	−3.0, −10.1, 13.1	−3.1, −9.8, 12.9	−2.9, −10.0, 12.9	
^{2}[Co(CO)$_4$]	^{13}C$_{ax}$	4.2	4.0	3.9	3.4	3.3	3.8	3.9	4.3	3.6
	^{13}C$_{eq}$[f]	8.3, −6.6, −1.7	8.1, −6.4, −1.7	8.3, −6.6, −1.7	9.7, −7.7, −1.9	9.7, −7.7, −2.0	12.8, −11.8, −1.0	12.7, −11.9, −0.8	14.0, −13.6, −0.4	
	^{17}O$_{ax}$	−4.1	−4.1	−4.2	−4.0	−4.1	−5.5	−5.8	−6.4	
	^{17}O$_{eq}$[f]	2.2, −10.2, 8.0	2.4, −10.1, 7.7	2.2, −10.0, 7.8	0.3, −10.0, 9.6	0.3, −10.1, 9.8	5.8, −23.7, 17.9	6.2, −25.0, 18.8	6.9, −38.0, 31.1	
^{2}CuO	^{17}O	−112.1	−111.9	−112.6	−121.2	−121.2	−126.1	−125.8	−126.2	
^{2}Cu(CO)$_3$	^{13}C[d]	−11.8, −13.8, 25.6	−11.9, −13.3, 25.2	−12.2, −13.4, 25.7	−10.5, −12.5, 23.1	−11.0, −12.3, 23.3	−8.2, −10.5,18.7	−8.3, −9.6, 17.9	−8.9, −9.8, 18.8	−12.3, −12.3, −24.6
	^{17}O[d]	16.2, 15.9, −32.2	15.8, 15.5, −31.3	15.8, 15.5, −31.3	16.5, 16.1, −32.6	16.0, 15.8, −31.8	15.9, 14.0, −29.9	15.7, 14.3, −30.0	15.7, 14.2, −30.0	

[a] Individual T_{ii} components are given for nonaxial tensors. [b] Experimental values are taken from the sources cited in the footnotes to Tables 8 and 10. [c] In Ne or Ar matrix, respectively. [d] Hyperfine tensor components are given in order: (1) along the metal−ligand bond, (2) normal to the metal−ligand bond, in the molecular plane, and (3) along the molecular *z*-axis. [e] Anisotropy experimentally not well defined, cf. discussion in ref 18. [f] Hyperfine tensor components are given in order: (1) along the metal−ligand bond, (2) normal to the metal−ligand bond and paralel to the *xy* plane, and (3) perpendicular to directions 1 and 2.

agreement with experiment than pure GGAs. A relatively large dependence on ν_c is also apparent for MnF and MnF_2.

A large dependence on ν_x is seen for the isotropic ^{13}C HFCCs of the axial ligands in $^2[Mn(CO)_5]$ and $^2[Fe(CO)_5]^+$. The exchange−correlation potential affects mainly the valence-shell spin polarization, and the direct SOMO contribution. The (smaller) dependencies on ν_x and ν_c for VO, TiN, and TiF_3 are also due to the valence-shell polarization and to SOMO contributions. Particularly large dependence on ν_{xc} is found in all cases with significant spin contamination problems, e.g., for MnO_3. Thus, the very large dependence of $A_{iso}(O)$ in MnO_3 on ν_x is probably an artifact of the large spin contamination with BH-type hybrid functionals (cf. section 7 and Table 9). Other examples are ^{13}C and nitrosyl ^{14}N HFCCs in $[Mn(CN)_5NO]^{2-}$, ^{13}C and nitride ^{14}N HFCCs in $[Mn(CN)_4N]^-$, and ^{13}C HFCCs in $[Co(CO)_4]$ (Table 10).

For most of the present systems, the theoretical values for A_{dip} of the ligands are very small, and often results with different functionals differ by less than 1 MHz. Agreement with the sparse experimental data appears reasonable in these cases. A larger dependence on ν_{xc} is seen for TiF_3, MnO, and MnF_2 (and also for cases with large spin contamination, cf. above). Thus, the ligand dipolar couplings in ^6MnO and $^6MnF_2$ increase when adding exact exchange.

9. Conclusions

The present study shows that the quantitative calculation of hyperfine coupling constants for transition metal systems is still a challenge to quantum chemistry, more so than for organic radicals. None of the density functionals investigated here may be considered to provide acceptable results for the whole range of transition metal species studied. For a number of particularly difficult systems, essentially none of the functionals provides satisfactory results.

There are various reasons why the HFCCs of transition metal systems present such difficulties. One of them is the very delicate core−shell spin polarization, which is in many cases the dominant pathway to create spin density at the metal nucleus. Even for an isolated transition metal atom (consider Mn^+ in section 5), we may understand why this type of spin polarization is so difficult to describe by present-day functionals. The spin polarization is mainly due to exchange interactions between singly occupied metal 3d orbitals and the outermost doubly occupied 3s- and 2s-type core shells. It is clear that these exchange interactions are strongly nonlocal (specific examples will be discussed elsewhere[25]) and thus difficult to account for with approaches derived from the local density approximation.[94] It is also clear that the description of such subtle spin-polarization effects is very different from the energy quantities that are currently used to fit the free parameters in the exchange−correlation functionals. The description of spin polarization is already nontrivial for organic π-radicals.[13,15,83] The spin polarization mechanisms in transition metal complexes are even more variable, and they involve not only the valence shell but also to a large extent the outermost core shells of the metal.

A second difficulty is connected to spin contamination. In several of the examples studied here, spin contamination became significant when exact exchange was mixed into ν_x. This led to a significant deterioration of the results. In some cases where spin polarization was underestimated at the GGA level, and where exact-exchange mixing would thus have been desirable to increase it, the dramatic onset of spin contamination made it impossible to improve the results with hybrid functionals. In some of the “limiting cases” discussed toward the end of section 7, spin contamination is already significant with pure GGA-type functionals. The spin contamination for the hybrid functionals is closely related to the well-known bias of unrestricted Hartree−Fock wave functions for higher spin multiplicities. Obviously, the spin contamination may be very pronounced for transition metal complexes (particularly so for 3d-metals!) due to the presence of low-lying excited states.

It is not clear how the magnitude of the spin polarization could be increased while avoiding significant spin contamination.[95] However, one may speculate that improved functionals might give increased core−shell spin polarization without exceedingly large valence-shell spin polarization (and thus spin contamination). Obviously, the description of valence spin polarization is also not trivial, even in cases with low spin contamination (cf. section 7). It seems likely that the desired functional would have to incorporate significantly less than 50% exact exchange. Generally, hyperfine coupling constants, in particular for transition metal systems, may turn out to be a particularly fruitful testing ground for new DFT (or alternative) approaches. In addition to the appreciable literature on organic molecules,[13,15,31] the hyperfine coupling constants of the 21 complexes studied in the present work should be useful as a benchmark set against which to calibrate new methods.

On the other hand, we should not judge even the present situation too pessimistically. For a significant number of complexes, the ca. 10−15% agreement with experimental isotropic metal HFCCs we were aiming for has been achieved with essentially all of the functionals (e.g., for ScO, TiN, TiO, VO, MnO, or MnF). In other subsets of molecules, the analysis of the electronic structure suggests the range of functionals (GGAs, B3-type, or BH-type hybrids) that might be most appropriate (as shown by the various examples discussed in this work). Careful selection of functionals is thus still expected to allow useful chemical applications in many areas, even though such an approach is obviously not completely satisfactory from a theoretical point of view. We expect that spin contamination is less pronounced for 4d or 5d transition metal complexes, and thus the choice of functional may also be somewhat less critical (on the other hand, relativistic effects will definitely have to be considered for heavy-atom systems, and we are presently developing approaches to do so).

The coupled cluster calculations we carried out for a subset of systems appear to be less influenced by such problems. Even in cases of significant spin contamination the results appeared to remain relatively stable. On the other hand, the computational effort involved presently makes such coupled-cluster approaches prohibitive for larger systems. Even for those di-, tri-, and tetraatomic complexes studied here, the large demand on the computational resources has not allowed us to truly saturate the basis sets with regard to higher angular momentum functions. There remains thus an urgent need for more economical approaches, and more accurate density functionals might offer the most practical route for improvement.

The present calculations also show conclusively that spin-polarization effects are nonnegligible for the metal dipolar couplings. This contrasts to the situation for main group compounds, where it is usually sufficient to take account of the direct SOMO spin densities to obtain good results for dipolar couplings.[13] The importance of spin polarization for transition metal dipolar hyperfine couplings arises from the presence of strongly polarizable semicore p-type orbitals (mainly the 3p orbitals for first-row transition metals), which have a very similar radial extent as the valence d-type SOMO orbitals. The importance of spin polarization for dipolar coupling constants of the metal had already been noted by Belanzoni et al., in their careful study of TiF_3.[17] In view of the importance of spin polarization, the widely used simplified models that derive the d or s character of the SOMO directly from the dipolar coupling constants should be viewed with caution in transition metal systems. More detailed analyses of spin-polarization mechanisms for transition metal hyperfine coupling constants will be given elsewhere.[25]

Acknowledgment. This work has been supported by Deutsche Forschungsgemeinschaft and by Fonds der Chemischen Industrie. Part of this work benefitted also from the graduate college "Moderne Methoden der magnetischen Resonanz" at Universität Stuttgart. We are grateful to Vladimir G. Malkin, Olga L. Malkina (Bratislava), Pavel Kubáček (Brno), and Dominik Munzar (Stuttgart) for helpful discussions. Jürgen Gauss (Mainz) kindly provided assistance with the ACES-II code. We also thank Evert-Jan Baerends (Amsterdam) for a preprint of ref 18 and Ernest R. Davidson for informing us about an error in ref 21 (cf. section 7).

References and Notes

(1) Abragam, A.; Bleaney, B. *Electron Paramagnetic Resonance of Transition Ions*; Clarendon Press: Oxford, 1970.

(2) Symons, M. C. R. *Chemical and Biochemical Aspects of Electron-Spin Resonance Spectroscopy*; Van Nostrand: New York, 1978.

(3) Atherton, N. M. *Principles of Electron Spin Resonance*; Prentice Hall: New York, 1993.

(4) Weil, J. A.; Bolton, J. R.; Wertz, J. E. *Electron Paramagnetic Resonance: Elementary Theory and Practical Applications*; Willey & Sons: New York, 1994.

(5) Carrington, A.; McLachlan, A. D. *Introduction to Magnetic Resonance with Applications to Chemistry and Chemical Physics*; Harper & Row: London, 1969.

(6) Weltner, W., Jr. *Magnetic Atoms and Molecules*; Van Nostrand: New York, 1983.

(7) McGarvey, B. R. In *Transition Metal Chemistry: A Series of Advances*; Carlin, R. L., Ed.; Marcel Dekker: New York, 1966; Vol 3., pp 89−201.

(8) Mabbs, F. E.; Collison, D. *Electron Paramagnetic Resonance of d Transition Metal Compounds*; Elsevier: Amsterdam, 1992.

(9) Mattar, S. M.; Hamilton, W. D.; Kingston, C. T. *Chem. Phys. Lett.* **1997**, *271*, 125.

(10) Mattar, S. M.; Kennedy, C. *Chem. Phys. Lett.* **1995**, *238*, 230.

(11) Mattar, S. M.; Doleman, B. J. *Chem. Phys. Lett.* **1993**, *216*, 369.

(12) Knight, L. B.; Babb, R.; Ray, M.; Banisaukas, T. J. III; Russon, L.; Dailey, R. S.; Davidson, E. R. *J. Chem. Phys.* **1996**, *105*, 10241.

(13) Engels, B.; Eriksson, L.; Lunell, S. *Adv. Quantum Chem.* **1996**, *27*, 297.

(14) Barone, V.; Fournier, R.; Mele, F.; Russo, N.; Adamo, C. *Chem. Phys. Lett.* **1995**, *237*, 189.

(15) Barone, V. In *Recent Advances in Density Functional Theory*; Chong, D. P., Ed.; World Scientific: Singapore, 1995; Part 1, p 287.

(16) Aarnts, M. P.; Wilms, M. P.; Peelen, K.; Fraanje, J.; Goubitz, K.; Hartl, F.; Stufkens, D. J.; Baerends, E. J.; Vlcek, A., Jr. *Inorg. Chem.* **1996**, *35*, 5468.

(17) Belanzoni, P.; Baerends, E. J.; van Asselt, S.; Langewen, P. B. *J. Phys. Chem.* **1995**, *99*, 13094.

(18) Belanzoni, P.; Baerends, E. J.; Gribnau, M *J. Phys. Chem. A* **1999**, *103*, 3732.

(19) van Lenthe, E.; van der Avoird, A.; Wormer, P. E. S. *J. Chem. Phys.* **1998**, *108*, 4783.

(20) Swann, J.; Westmoreland, T. D. *Inorg. Chem.* **1997**, *36*, 5348.

(21) Knight, L. B.; Kaup, J. G.; Petzoldt, B.; Ayyad, R.; Ghanty, T. K.; Davidson, E. R. *J. Chem. Phys.* **1999**, *110*, 5658.

(22) Geurts, P. J. M.; Bouten, P. C. P.; van der Avoird, A. *J. Chem. Phys* **1980**, *73*, 1306.

(23) Case, D. A.; Karplus, M. *J. Am. Chem. Soc.* **1977**, *99*, 6182.

(24) Weber, J.; Goursot, A.; Pénigault, E.; Ammeter, J. H.; Bachmann, J. *J. Am. Chem. Soc.* **1982**, *104*, 1491.

(25) Munzarová, M.; Kaupp, M., in preparation.

(26) Harriman, J. E. *Theoretical Foundations of Electron Spin Resonance,* Academic Press: New York, 1978.

(27) Childs, W. J. *Phys. Reports* **1992**, *211*, 114.

(28) Childs, J.; Steimle, T. C. *J. Phys. Chem.* **1988**, *88*, 6168.

(29) Fletcher, D. A.; Surlock, C. T.; Jung, K. Y.; Steimle, T. C. *J. Chem. Phys.* **1993**, *99*, 4288.

(30) Carrington, A. *Microwave Spectroscopy of Free Radicals*; Academic Press: New York, 1974.

(31) Malkin, V. G.; Malkina, O. L.; Eriksson, L. A.; Salahub, D. R. In *Modern Density Functional Theory: A Tool for Chemistry, Vol. 2 of Theoretical and Computational Chemistry*; Politzer, P., Seminario, J. M., Eds.; Elsevier: Amsterdam, The Nederlands, 1995; pp 273−347.

(32) Kasai, P. H. *J. Chem. Phys.* **1968**, *49*, 4979.

(33) Cheung, A. S-C.; Hansen, R. C.; Merer, A. J. *J. Mol. Spectrosc.* **1982**, *91*, 165.

(34) Weltner, W., Jr.; McLeod, D., Jr.; Kasai, P. *J. Chem. Phys.* **1967**, *46*, 3172.

(35) Baumann, C. A.; Van Zee, R. J.; Weltner, W., Jr. *J. Phys. Chem.* **1982**, *86*, 5084.

(36) Namiki, K.; Saito, S. *J. Chem. Phys.* **1997**, *107*, 8848.

(37) Varberg, D.; Field, R. W.; Merer, A. J. *J. Chem. Phys.* **1991**, *95*, 1563.

(38) Morton, J. R.; Preston, K. F. *J. Chem. Phys.* **1984**, *81*, 5775.

(39) Frisch, M. J.; Trucks, G. W.; Schlegel, H. B.; Gill, P. M. W.; Johnson, B. G.; Robb, M. A.; Cheeseman, J. R.; Keith, T.; Petersson, G. A.; Montgomery, J. A.; Raghavachari, K.; Al-Laham, M. A.; Zakrzewski, V. G.; Ortiz, J. V.; Foresman, J. B.; Peng, C. Y.; Ayala, P. Y.; Chen, W.; Wong, M. W.; Andres, J. L.; Replogle, E. S.; Gomperts, R.; Martin, R. L.; Fox, D. J.; Binkley, J. S.; Defrees, D. J.; Baker, J.; Stewart, J. P.; Head-Gordon, M.; Gonzalez, C.; Pople, J. A. *Gaussian 94* (revision E.2); Gaussian, Inc.: Pittsburgh, PA, 1995.

(40) Dolg, M.; Wedig, U.; Stoll, H.; Preuss, H. *J. Chem. Phys.* **1987**, *86*, 866.

(41) (a) Bergner, A.; Dolg, M.; Küchle, W.; Stoll, H.; Preuss, H. *Mol. Phys.* **1993**, *80*, 1431. (b) d-Type polarization functions have been taken from*: Gaussian Basis Sets for Molecular Calculations*; Huzinaga, S., Ed.; Elsevier: New York, 1984.

(42) Dunning, T. H.; Hay, H. In *Methods of Electronic Structure Theory, Vol. 3 of Modern Theoretical Chemistry*; Schaefer, H. F., III, Ed.; Plenum Press: New York, 1977.

(43) Ehlers, A. W.; Böhme, M.; Dapprich, S.; Gobbi, A.; Höllwarth, A.; Jonas, V.; Köhler, K. F.; Stegmann, R.; Veldkamp, A.; Frenking, G. *Chem. Phys. Lett.* **1993**, *208*, 111.

(44) DeVore, C.; Weltner, W., Jr. *J. Am. Chem. Soc.* **1977**, *99*, 4700.

(45) Ferrante, F.; Wilkerson, J. L.; Graham, W. R. M.; Weltner, W., Jr. *J. Chem. Phys.* **1977**, *67*, 5904.

(46) Kasai, P. H.; Jones, P. M. *J. Am. Chem. Soc.* **1985**, *107*, 818.

(47) Chenier, J. H. B.; Hampson, C. A.; Howard, J. A.; Mile, B. *J. Phys. Chem.* **1989**, *93*, 114.

(48) Hastie, J. W.; Hauge, R. H.; Margrave, L. *J. Chem. Phys.* **1969**, *51*, 2648.

(49) Huber, H.; Kündig, E. P.; Moskovits, M.; Ozin, G. A. *J. Am. Chem. Soc.* **1975**, *97*, 2097.

(50) Fairhust, S. A.; Morton, J. R.; Preston, K. F. *J. Magn. Res.* **1983**, *55*, 453.

(51) Morton, J. R.; Preston, K. F. *J. Chem. Phys.* **1984**, *81*, 5775.

(52) Fairhust, S. A.; Morton, J. R.; Preston, K. F. *Chem. Phys. Lett* **1984**, *104*, 112.

(53) Buschmann, W. E.; Arif, A. M.; Miller, J. S. *Angew. Chem., Int. Ed. Engl.* **1998**, *110*, 813.

(54) Symons, M. C. R. *Organometallics* **1982**, *1*, 834.

(55) Lionel, T.; Morton, J. R.; Preston, K. F. *J. Chem. Phys.* **1982**, *76*, 234.

(56) Rosa, A.; Ehlers, A. W.; Baerends, E. J.; Snijders, J. G.; te Velde, G. *J. Phys. Chem.* **1996**, *100*, 5690.

(57) Ricca, A.; Bauschlicher, C. W., Jr. *J. Phys. Chem.* **1994**, *98*, 12899.

(58) Bendix, J.; Meyer, K.; Weyhermüller, T.; Bill, E.; Metzler-Nolte, N.; Wieghart, K. *Inorg. Chem.* **1998**, *37*, 1767.

(59) Pink, M.; Billig, R. *Z. Kristallogr.* **1996**, *211*, 203.

(60) Becke, A. D. *Phys. Rev. A* **1988**, *38*, 3098.

(61) Lee, C.; Yang, W.; Parr, G. R. *Phys, Rev. B* **1988**, *37*, 785. Miehlich, B.; Savin, A.; Stoll, H.; Preuss, H. *Chem. Phys. Lett.* **1989**, *157*, 200.

(62) Perdew, J. P.; Wang, Y. *Phys. Rev. B* **1986**, *33*, 8822. Perdew, J. P.; Wang, Y. *Phys. Rev. B* **1986**, *34*, 7406.

(63) Perdew, J. P. *Physica B* **1992**, *172*, 1. Perdew, J. P. In *Electronic Structure of Solids '91*; Ziesche, P., Eschring, H., Eds.; Akademie Verlag: Berlin, 1991. Perdew, J. P.; Wang, Y. *Phys. Rev. B* **1992**, *45*, 13244.

(64) Becke, A. D. *J. Chem. Phys.* **1993**, *98*, 5648.

(65) Becke, A. D. *J. Chem. Phys.* **1993**, *98*, 1372.

(66) Gianturco, A.; de Larra-Castels, M. P.; *Chem. Phys.* **1996**, *208*, 25. Braida, B.; Hiberty, P. C.; Savin, A. *J. Phys. Chem. A* **1988**, *102*, 7872.

(67) Holthausen, M. C.; Heinemann, C.; Cornehl, H. H.; Koch, W.; Schwarz H. *J. Chem. Phys.* **1995**, *102*, 4931.

(68) Stanton, J. F.; Gauss, J.; Watts, J. D.; Lauderdale, W. J.; Bartlett, R. J.; ACES−II program; University of Florida: Gainesville, 1994. Prof. J. Gauss (Universität Mainz) provided a modified version. For the underlying relaxed-density matrix MBPT/CC approach, see, e.g., Salter, E. A.; Trucks,

G. W.; Bartlett, R. J. *J. Chem. Phys.* **1989**, *90*, 1752. Perreira, S. A.; Watts, J. D.; Bartlett, R. J. *J. Chem. Phys.* **1994**, *100*, 1425.

(69) Schäfer, A.; Horn, H.; Ahlrichs, R. *J. Chem. Phys* **1992**, *97*, 2571.

(70) Kutzelnigg, W.; Fleischer, U.; Schindler, M. In *NMR−Basic Principles and Progress*; Springer-Verlag: Heidelberg, 1990; Vol. 23, p 165.

(71) Pou-Amerigo, R.; Merchan, M.; Nebot-Gil, I.; Widmark, P. O.; Roos, B. *Theor. Chim. Acta* **1995**, *92*, 149, based on the (20s, 12p, 9d) primitives of Partridge, H. *J. Chem. Phys*. **1989**, *90*, 1043.

(72) Bauschlicher, C. W., Jr.; Langhoff, S. R.; Barnes, L. A. *J. Chem. Phys*. **1989**, *91*, 2399.

(73) Cf. *Extensible Computational Chemistry Environment Basis Set Database, Version 1.0*; Molecular Science Computing Facility: Pacific Northwest Laboratory.

(74) Pyykkö, P.; Pajanne, E.; Inokuti, M. *Int. J. Quantum Chem.* **1973**, *7*, 785.

(75) Harriman, J. E. *Theoretical Foundations of Electron Spin Resonance*; Academic Press: New York, 1978.

(76) Abragam, A.; Pryce, M. H. L. *Proc. R. Soc. London A* **1951**, *205*, 135.

(77) Purvis, G. D., III; Sekino, H.; Bartlett, R. J. *Collect. Czech. Chem. Commun.* **1988**, *53*, 2203.

(78) Laidig, W. D.; Purvis, G. D., III; Bartlett, R. J. *Int. J. Quantum Chem. Symp.* **1982**, *16*, 561.

(79) Eriksson, L. A.; Malkina, O. L.; Malkin, V. G.; Salahub, D. R. *J. Chem. Phys.* **1994**, *100*, 5066. Eriksson, L. A.; Malkina, O. L.; Malkin, V. G.; Salahub, D. R. *Int. J. Quantum Chem.* **1994**, *52*, 879.

(80) See also, e.g., Chipman, D. M. *J. Chem. Phys.* **1989**, *91*, 5455. Chipman, D. M. *Theor. Chim. Acta* **1989**, *76*, 73. Engels, B.; Peyerimhoff, S. D. *J. Phys. B: At. Mol. Opt. Phys.* **1988**, *21*, 3459. Engels, B.; Peyerimhoff, S. D. *Mol. Phys.* **1989**, *67*, 583.

(81) We note that the metal 3s-shell provides a positive core−shell spin-polarization contribution to the metal HFCC, whereas the 2s-shell provides an even larger negative contribution. This is consistent with previous interpretations, see refs 1 and 3. Compare also: Freeman, A. J.; Watson, R. E. In *Magnetism;* Rado, G. T., Suhl, H., Eds.; Academic Press: New York, 1965; Volume IIA, p 167. Watson, R. E.; Freeman, A. J. In *Hyperfine Interactions*; Freeman, A. J., Fraenkel, R. D., Eds.; Academic Press: New York, 1967; p 53, as well as refs 23 and 24.

(82) These $<S^2>$ values pertain to the Kohn−Sham wave function, i.e., to the noninteracting reference system rather than to the real system. Such data are nevertheless expected to give a reasonable and useful representation for the real system as well (see, e.g., Baker, J.; Scheiner, A.; Andzelm, J. *Chem. Phys. Lett.* **1993**, *216*, 380).

(83) Suter, H. U.; Pless, V.; Ernzerhof, M.; Engels, B. *Chem. Phys. Lett.* **1994**, *230*, 398.

(84) Note, however, that there may be significant differences even between different GGA functionals.[13,15,31,83]

(85) Note however, that for π-type radicals spin polarization is important.[13−15,83] Indeed, it appears that in many cases even B3LYP underestimates this spin polarization. See also, e.g., Carmichael, I. *J. Phys. Chem. A* **1997**, *101*, 4633.

(86) We note that a similar situation pertains presently for the application of DFT methods to the calculation of NMR chemical shifts for transition metal nuclei. For reviews see, e.g., Bühl, M.; Kaupp, M.; Malkin, V. G.; Malkina, O. L. *J. Comput. Chem.* **1999**, *20*, 91. Kaupp, M.; Malkina, O. L.; Malkin, V. G. In *Encyclopedia of Computational Chemistry*; Schleyer, P. v. R., Ed.; Wiley-Interscience: New York, 1998, pp 1857ff.

(87) Davidson, E. R., personal communication.

(88) $[Co(CO)_4]$ may be considered a typical case of a Jahn−Teller distortion within a nonrelativistic framework.[88a] Spin−orbit coupling is, however, expected to lift the degeneracy of the ground state.[88b] (a) See, e.g., Burdett, J. K. *J. Chem. Soc., Faraday Trans. 2* **1974**, *70*, 1599. (b) See, e.g., Hanlan, L. A., Huber, H.; Kündig, E. P.; McGarvey, B. R.; Ozin, G. A. *J. Am. Chem. Soc.* **1975**, *97*, 7054.

(89) Hippe, D.; Peyerimhoff, S. D. *Mol. Phys*. **1992**, *76*, 293.

(90) a) Salahub, D. R.; Fournier, R.; Mlynarski, P.; Papai, I.; St-Amant, A.; Ushio, J. In *Density Functional Methods in Chemistry*; Labanowski, J., Andzelm, J., Eds.; Springer: New York, 1991. (b) St-Amant, A.; Salahub, D. R. *Chem. Phys. Lett.* **1990**, *169*, 387.

(91) Langhoff, S. R.; Bauschlicher, C. W., Jr. *Chem. Phys. Lett.* **1986**, *124*, 241.

(92) Huber, K. P.; Herzberg, G. *Molecular Spectra and Molecular Structure. IV. Constants of Diatomic Molecules*; Van Nostrand: New York, 1979.

(93) Bauschlicher C. W., Jr.; Maitre, P. *Theor. Chim. Acta* **1995**, *90*, 189.

(94) In this study we have concentrated on GGA exchange functionals derived from Becke's 1986 *ansatz*. Some differences may already be expected when using other GGA approaches.[31,79]

(95) In principle, one might remove the spin contaminants by spin projection techniques. However, the justification for doing so is doubtful. For a lucid discussion, see e.g., Chipman, D. M. *Theor. Chim. Acta* **1992**, *82*, 93.